Article

Not peer-reviewed version

Effect of Temperature Over the Growth and Biofilm Formation of the Thermotolerant *Aspergillus flavus*

José Alejandro Hernández-Benítez , Brenda Nallely Santos-Ocampo , Daniel Genaro Rosas-Ramírez , Adrian Ramírez-Granillo , Luis Antonio Bautista-Hernández , Víctor Manuel Bautista-de Lucio , Nestor Octavio Pérez * , Aída Verónica Rodríguez-Tovar *

Posted Date: 13 September 2024

doi: 10.20944/preprints202409.1082.v1

Keywords: *Aspergillus flavus*; biofilm; thermotolerant; extracellular matrix; lipid droplets; antifungal susceptibility

Article

Effect of Temperature Over the Growth and Biofilm Formation of the Thermotolerant *Aspergillus flavus*

José Alejandro Hernández-Benítez [1], Brenda Nallely Santos-Ocampo [1], Daniel Genaro Rosas-Ramírez [2], Adrián Ramírez-Granillo [1], Luis Antonio Bautista-Hernández [3], Víctor Manuel Bautista-de Lucio [3], Néstor Octavio Pérez [4,*] and Aída Verónica Rodríguez-Tovar [1,*]

[1] Departamento de Microbiología, Escuela Nacional de Ciencias Biológicas, Instituto Politécnico Nacional, Prol. Carpio y Plan de Ayala s/n Col. Casco de Santo Tomás, Alcaldía Miguel Hidalgo, C.P. 11340, Ciudad de México, México

[2] Departamento de Química de Biomacromoléculas Instituto de Química, Universidad Nacional Autónoma de México, Av. Universidad 3000, Circuito Exterior s/n, Ciudad Universitaria, Alcaldía Coyoacán, C.P. 04510, Ciudad de México, México

[3] Unidad de Investigación del Instituto de Oftalmología "Fundación de Asistencia Privada Conde de Valenciana I.A.P.", Chimalpopoca 14, Col. Obrera, Alcaldía Cuahutémoc, C.P. 06800, Ciudad de México, México

[4] Departamento de Investigación y Desarrollo, Probiomed, S.A. de C.V., Cruce de Carreteras Acatzingo-Zumahuacan s/n, Tenancingo, C.P. 52400, Estado de México, México

* Correspondence: nestor.perez@probiomed.com.mx (N.O.P.); avrodriguez@ipn.mx (A.V.R.-T.), Tel.: +52 5557296000 Ext. 52379 (A.V.R.-T.)

Abstract: *Aspergillus flavus* is a medically relevant fungus, particularly in tropical regions. Thermotolerance is a key virulence factor as an opportunistic pathogen, as well as its ability to form biofilms, which can impact therapeutic outcomes. To know how temperature affects the growth and biofilm formation of an *A. flavus* isolate, we assessed its growth on solid media and described the morphological changes during conidial germination. We also examined formation and composition of in vitro biofilm incubated at different temperatures and compared the susceptibility of planktonic and biofilm cells to antifungal agents. Our results showed that temperature promotes conidiation on solid media. The radial growth was higher at 28 °C, but total conidia was higher at 37 °C, however, conidial density was stronger at 42 °C. Moreover, incubation at 37 °C accelerates conidial germination and is the optimal temperature for biofilm formation. We described four distinct phases in *A. flavus* biofilm development: initiation (0-12h), consolidation (12-48h), maturation (48-72h), and dispersion (>72h), where the presence of aspergillar heads was notable at 42 °C. Carbohydrates and proteins are the main components of the extracellular matrix. We observed lipid droplets within the biofilm hyphae, and mature biofilms are resistant to amphotericin B and itraconazole, with MICs exceeding 16 μg/mL for both antifungals, regardless of the incubation temperature.

Keywords: *Aspergillus flavus*; biofilm; thermotolerant; extracellular matrix; lipid droplets; antifungal susceptibility

1. Introduction

The filamentous genus *Aspergillus* is composed of more than 200 species of ubiquitous fungi that can be found in air, water, and soil. They can develop as saprobes on decaying organic matter [1]. Nevertheless, species grouped in the *Fumigati*, *Flavi*, *Nigri*, *Terrei*, and *Nidulantes* sections have been described as opportunistic pathogens of humans and animals. Among these, *Aspergillus fumigatus* is the main medically relevant species and the principal etiological agent of invasive pulmonary aspergillosis (IPA) [2]. *Aspergillus flavus* is the second most frequently associated species with IPA, especially in warm-weather countries [3,4]. Moreover, the pathogenic spectrum of *A. flavus* is broader and extends beyond pulmonary aspergillosis, including fungal keratitis [5–7], aspergilloma [8–11]

 doi:10.20944/preprints202409.1082.v1

and skin infections [12–14]. Furthermore, *A. flavus* is a prominent source of fungal contamination in grain and corn warehouses, resulting in economic losses by product deterioration and a health risk to human and animal due to its ability to produce mycotoxins, [15–18]. The ability to grow across a broad range of temperatures is one of the virulence factors of the *Aspergillus* genus. This allows them to be found at diverse geographical locations [19] and can favor their capacity to colonize, germinate [20], and develop inside mammalian respiratory tracts, acting as pathogens [21,22]. In fact, the relationship between tropical climatic conditions and the prevalence of infections associated with *A. flavus* has been documented [23,24]. This phenomenon is attributed to the adaptability of this fungus, whether in decaying organic matter or inside the human body, involving changes in genetic regulation and subsequent morphophysiological adaptations [25], such as expression of heat shock protein [26], the accumulation of solutes [27], and remodeling of the cell wall [28]. Another characteristic that highlights the adaptive capacity of microorganisms, is their ability to form biofilm [29]. Biofilm formation and its role in virulence and resistance to various factors, including antimicrobial therapy and the immune system, have been extensively documented in fungi such as *Candida albicans* [30,31] and *A. fumigatus* [32,33]. Due to its medical importance, significant efforts have been directed towards the characterization of biofilm in these models. However, the rise of opportunistic fungal infections associated with emerging or re-emerging fungi is a serious concern, particularly in the context of climate change, which may drive the adaptation of diverse microorganisms to adverse conditions, such as fluctuations in temperature [34–36]. The aim of this work was to investigate the effect of temperature on the development of *A. flavus*, isolated from a hospital environment. We characterized the growth on solid media and the biofilm formation capacity at three different temperatures. We assessed its germination rate, biomass production, as well as the architecture and composition of the biofilm and its response to antifungal agents.

2. Materials and Methods

2.1. Biological Material and Identification

The strain of *Aspergillus sp.* used was isolated from a hospital setting, (kindly provided by MSc Jesús Reséndiz Sánchez, from the Hospital Infantil de México "Federico Gómez"). It was grown in Sabouraud dextrose agar (SDA) (DIBICO™, Cuautitlán Izcalli, State of Mexico, Mexico), potato dextrose agar (PDA) (BD Bioxón™, Cuautitlán Izcalli, State of Mexico, Mexico) and Czapek Dox agar (CPK) (Sigma-Aldrich, St. Louis, MO, USA) at 28 °C for 7 days to describe its colonial morphology; the description of asexual and sexual reproductive structures was performed using microculture at 28 °C for 7 days.

Molecular identification was performed through genomic DNA extraction following the protocol described by Rodríguez-Tovar *et al.*, [37], followed by PCR amplification of ITS region and β-tubulin encoding gene. The amplification was conducted using an Axygen™ MaxyGene II thermal cycler (Corning, NY, USA), with a reaction mixture containing 100 ng DNA template, 20 pmol of each primers: ITS1 (5′-TCCGTAGGTGAACCTGCGG-3′) and ITS4 (5′-TCCTCCGCTTATTGATATGC-3′) for ITS region [38]; and Bt2a (5′-GGTAACCAAATCGGTGCTGCTTTC-3′) and Bt2b (5′-ACCCTCAGTCTAGTGACCCTTGGC-3′) for β-tubulin [39], 25 µL 2X PCR SuperMix™ (GeneDirex, Taoyuan, Taiwan), in a final volume of 50 µL. The following conditions were used: an initial denaturation step at 95 °C for 10 min, followed by 35 cycles of 1 min at 95 °C, 1 minute at 56.7 °C for ITS and 55 °C for β-tubulin, and 1 min at 72 °C, with a final extension step at 72 °C for 10 min. The PCR products were sequenced in MacroGen Inc. (Seoul, South Korea). Sequences were edited and aligned using BioEdit (version 7.2.5) and the Clustal Omega server (https://www.ebi.ac.uk/jdispatcher/msa/clustalo), respectively. Subsequently, sequences were analyzed using BLASTn (https://blast.ncbi.nlm.nih.gov/), and a phylogenetic tree was constructed using the Neighbor-Joining method in MEGA 11 (version 11.0.8).

2.2. Aspergillus flavus MMe18 Growth at Different Temperatures

 doi:10.20944/preprints202409.1082.v1

The strain was identified as *A. flavus* MMe18 and was grown on PDA medium at 28 °C for 7 days. Then, conidia were harvested using 1X phosphate-buffered saline (PBS) (NaCl 8 g, KCl 0.2 g, NaH_2PO_4 1.37 g, KH_2PO_4 0.24 g) with 0.1% Tween 20 (Hycel de Mexico, Zapopan, Jalisco, Mexico). Conidial suspension was counted using a hemocytometer and adjusted to a concentration of $1x10^6$ conidia/mL in 1X PBS. The fungal inoculum was spotted onto Petri dishes containing PDA, SDA and CPK, and incubated at 28 °C, 37 °C and 42 °C for 7 days. Colony diameter, total conidia and the conidia-to-colony area ratio were determined at the end of the incubation period by triplicate. For subsequent experiments, these conditions of fungal inoculum, culture medium, and incubation temperature were used, except where otherwise noted.

2.3. Germination of Aspergillus flavus MMe18 Conidia

A fresh conidial suspension was adjusted at $1x10^6$ conidia/mL in supplemented RPMI 1640 medium (Gibco™, Thermo Fisher Scientific, Waltham, MA, USA). The adjusted inoculum was seeded into 12-well polystyrene plates (Santa Cruz Biotechnology, Dallas, Texas, USA), and incubated at 28 °C, 37 °C, and 42 °C. Fungal development was monitored throughout 10 hours using an inverted microscope (Primovert, Zeiss, Jena, Germany) at 400x total magnification. The germination percentage was determined by counting both germinated and non-germinated conidia. A two-way ANOVA, and the Holm-Sidak multiple comparisons test, were performed using GraphPad Prism (version 9.5.0), statistical significance is indicated by [*, $p<0.05$].

Metabolic activity during conidial germination was assessed using the MTT method, as described by Córdova-Alcántara et al. [40]. Fungal inoculum adjusted at $1x10^6$ conidia/mL was seeded into 96-well polystyrene plates (Nunc™ Thermo Scientific™, Waltham, MA, USA), and incubated at 28 °C, 37 °C, and 42 °C. After 4 h, 6 h, 8 h, and 10 h, the supernatant was removed, and 100 µL of 0.3% MTT (Invitrogen™, Thermo Fisher Scientific, Waltham, MA, USA) and 100 µL of 1X PBS were added and incubated at 37 °C in the dark for 2 h. Afterwards, the supernatant was removed, and 100 µL of dimethyl sulfoxide (DMSO) (Honeywell, Morrison, NJ, USA**)** and 25 µL of 0.1 M glycine buffer (pH 10.2) were added and incubated at room temperature for 15 minutes with mild shaking. Absorbance was measured using a microplate reader (UT-2100C MRC Laboratory Instruments, Holon, Israel) at a wavelength of 450 nm. Differences in absorbance between temperatures were analyzed by two-way ANOVA, followed by the Holm-Sidak multiple comparisons test, using GraphPad Prism (version 9.5.0), statistical significance is indicated by [*, $p<0.05$].

2.4. Aspergillus flavus MMe18 In Vitro Biofilm Formation

The conidial suspension was adjusted at $1x10^6$ conidia/mL in supplemented RPMI 1640 medium, as previously described. The biofilm was established as follows: 200 µL of the conidial suspension were added to each well in a 96-well polystyrene plate and incubated at 28 °C, 37 °C, and 42 °C for 4 h to allow the adherence phase. Then, the supernatant was removed and replaced with fresh RPMI 1640 medium. Biomass was quantified at each temperature over 72 h following the method described by Christensen et al. [41] and modified by Peeters et al. [42] and Ramírez-Granillo et al. [43]. After incubation, the supernatant was removed, and the biofilm was rinsed twice with 1X PBS, fixed with methanol, and stained with 0.005% crystal violet (CV). The dye crystals bound to the biofilm were dissolved using 33% (v/v) acetic acid, and the absorbance was measured using a microwell reader at a wavelength of 630 nm. Differences in absorbance were analyzed by two-way ANOVA and the Holm-Sidak multiple comparisons test, using GraphPad Prism (version 9.5.0).

Additionally, we studied the biofilm morphology by 0.005% CV staining and observed using an inverted microscope. And we determined the biofilm weight by establishing the biofilm in a 6-well polystyrene plate (Ultra Cruz™, Santa Cruz Biotechnology, Dallas, Texas, USA) and incubating at 28 °C, 37 °C, and 42 °C for 48 h. After this period, the supernatant was discarded, and the biomass was rinsed twice with 1X PBS, freeze-dried, and weighed.

2.5. Biofilm aRchitecture of Aspergillus flavus MMe18

 doi:10.20944/preprints202409.1082.v1

The fungal biofilm was established as described previously in 12-well polystyrene plates and incubated at 28 °C, 37 °C, and 42 °C. Observations were made using scanning electron microscopy (SEM) at 4 h, 8 h, 12 h, 24 h, 48 h, and 72 h. After each incubation period, the supernatant was discarded, and the biofilm was rinsed with 1X PBS, then fixed with 2.5% glutaraldehyde (Sigma-Aldrich, St. Louis, MO, USA) for 2 h, rinsed twice, and post-fixed with 1% osmium tetroxide (Sigma-Aldrich, St. Louis, MO, USA) for 2 h. Following the fixation and post fixation processes, samples were rinsed again, dehydrated with increasing concentrations of ethanol, and finally dried to the critical point using 1,1,1,3,3,3-hexamethyldisilazane (Electron Microscopy Sciences, Hatfield, PA, USA).

Samples were coated with ionized gold for 50 sec at 5.0 kV and 10 mA, and observed using SEM (FEI Quanta 3D FEG Dual Beam, FEI Company, Oregon, USA) at the Dual Beam Scanning Electron Microscopy Laboratory, and (JSM-7800F, JEOL Ltd., Tokio, Japan) at the High-Resolution Scanning Electron Microscopy Laboratory of the Nanosciences, Micro and Nanotechnologies Centre at the National Polytechnic Institute (CNMN-IPN), Mexico City. The samples were visualized according to schedule appointments in the CNMN-IPN.

2.6. Biochemical Composition of the Extracellular Matrix

The biofilm of *A. flavus* MMe18 was established as previously described on sterile glass coverslips (Velab™ Mexico, Mexico) placed at the bottom of a well in a 12-well polystyrene plate and incubated until the maturation phase (48 h) at 28 °C, 37 °C, and 42 °C. After this period, the supernatant was removed, and the biofilm was rinsed twice with 1X PBS. The samples were fixed with 4% paraformaldehyde (Sigma-Aldrich, St. Louis, MO, USA) for 2 h. Afterwards, biofilm was rinsed twice and covered with different mixtures of fluorochromes: M1: 1 g/L calcofluor white (CW, blue) (Sigma-Aldrich, St. Louis, MO, USA) + 10x Flamingo™ (green) (Biorad, CA, EUA), to label chitin and proteins, respectively; and M2: 1 mg/mL concanavalin A (ConA, green) (Sigma-Aldrich, St. Louis, MO, USA) + 100 µg/mL propidium iodide (PI, red), to label carbohydrates and extracellular DNA (eDNA), respectively. The presence of lipids in the biofilm was studied by staining with 10 mg/L Nile red (NR, orange) (Sigma-Aldrich, St. Louis, MO, USA). All samples were observed using an epifluorescence microscope (LSM Carl Zeiss, Germany) at the Ocular Microbiology and Proteomics Laboratory of the Ophthalmology Institute "Fundación Conde de Valenciana", Mexico City. The filters used were BC: 355-433 nm; Flamingo™: 512-535 nm; ConA: 495-519 nm; PI: 543-560 nm; NR: 543-560 nm.

Additionally, mature biofilms of *A. flavus* were stained with Sudan Black B and examined using brightfield microscopy (Sigma-Aldrich, St. Louis, MO, USA). After incubation, the supernatant was removed, and the biofilms were washed with 1X PBS. Then, stained with 0.5% Sudan black B in 70% ethanol, and dried at 50 °C for 20 minutes. Excess dye was removed with 70% ethanol, followed by counterstaining with 0.5% safranin. The samples were rinsed with distilled water, air-dried, and observed (PrimoStar, Zeiss, Jena, Germany).

To assess whether biofilm density varies with temperature, mature biofilms were stained with calcofluor white and analyzed using a confocal laser scanning microscope (CLSM) at the Multiphoton-Confocal Microscopy Laboratory of the CNMN-IPN, Mexico City.

2.7. Antifungal Susceptibility Profile of A. flavus MMe18 at Different Temperatures

The Minimum Inhibitory Concentration (MIC) of amphotericin B (AFB) and itraconazole (ITR) against both planktonic and biofilm fungal cells was determined at three temperatures. For planktonic determination, we followed the broth microdilution method for filamentous fungi described in the M38-A document [46] of the Clinical and Laboratory Standards Institute (CLSI). The polystyrene plates were incubated at 28 °C, 37 °C, and 42 °C. Results were determined spectrophotometrically after 48 h of incubation using a microplate reader at a wavelength of 405 nm with agitation. The MIC of both antifungals was considered as the lowest concentration that completely inhibits fungal growth.

For antibiofilm activity, the biofilm was established as previously described in a 96-well plate and incubated at different temperatures. After 12, 24, and 48 h of incubation, the supernatant was

 doi:10.20944/preprints202409.1082.v1

removed, and the preformed biofilm was exposed to the antifungals. The plates were then incubated until they reached a total of 72 h of incubation. Metabolic activity was measured with the MTT method.

3. Results

3.1. Morphological and Molecular Identification

The *Aspergillus sp.* isolate was cultured on different media and incubated at 28 °C, 37 °C, and 42 °C for 5 days, as shown in **Figure 1a**. The colonies exhibited a flat surface and downy texture, with light green to yellow coloration and a white halo at the border. No diffusible pigmentation was observed on the reverse side of the colonies. Notably, in SDA medium, the colonies produced a considerable number of dark sclerotia, each larger than 400 µm. Therefore, we suggest that its morphotype is L-type (**Figure 1b**). Microscopically, the fungus exhibits conidiophores with partially rounded conidial heads, from which uniseriate phialides and chains of conidia are arranged at an angle close to 360° (**Figure 1c**). Molecular identification was performed by sequencing and aligning the ITS1-5.8S-ITS2 rDNA fragment, with accession number **PQ269296**. The phylogenetic tree constructed using the Neighbor-Joining method (**Figure 1d**) shows that this *Aspergillus flavus* strain is grouped within the *A. flavus*-clade, along with other *A. flavus* and *A. parasiticus* isolates. Furthermore, these taxa are situated within the *Flavi* section, which includes *A. tamarii*. It was supported by constructing another phylogenetic tree using a fragment of the β-tubulin gene **(PQ306549)** (**Figure S1**). For subsequent experiments, the *A. flavus* isolate will be referred as *A. flavus* MMe18.

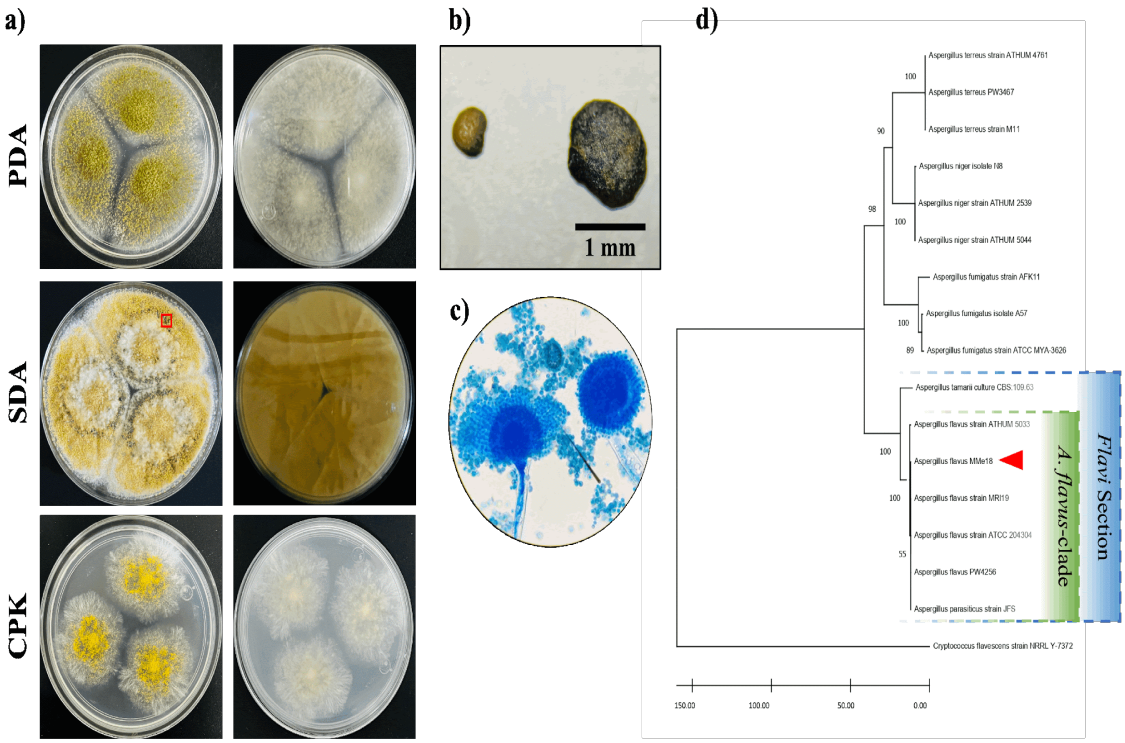

Figure 1. Identification of *Aspergillus flavus* MMe18. ***a)*** Macroscopic identification: front and back views of *Aspergillus flavus* MMe18 grown at 28 °C for 5 days on PDA, SDA and Czapek agar (CPK). There are downy texture colonies with light green to yellow on the surface and no diffusible pigmentation, ***b)*** sclerotia are prominently visible in SDA medium; and ***c)*** microscopic identification: observed at 1000x magnification with lactophenol cotton blue stain showing partially rounded conidial heads and uniseriate phialides from which chains of round conidia develop; ***d)*** ITS Neighbor-Joining phylogenetic tree with a bootstrap value of 1000, grouped isolated MMe18 within the *A. flavus*-clade in the *Flavi* section.

 doi:10.20944/preprints202409.1082.v1

3.2. Optimal Growth Conditions for Aspergillus flavus

The development of *A. flavus* MMe18 in different culture media and at different incubation temperatures was quantified by measuring colony diameter (**Figure 2a**), total conidia count (**Figure 2b**), and the conidia-to-colony area ratio (**Figure 2c**) after 7 days of incubation. The optimal temperature for radial growth was 28 °C for PDA and SDA, but 37 °C for CPK. Notably, this fungus demonstrated the capacity to grow even at 42 °C, a temperature at which colony diameter decreased across all media, but conidial counts remained higher than 10^7 conidia/mL, being SDA the lowest. Regardless of the culture medium, the conidia-to-colony area ratio increased with temperature, but in SDA medium, were we saw a decreased at 42 °C. These observations suggest that the conidiation rate may not be directly correlated with radial growth, but rather with the thermal stress imposed on the fungus at temperatures above its optimal range and the media used. These results confirm that *A. flavus* MMe18 is thermotolerant.

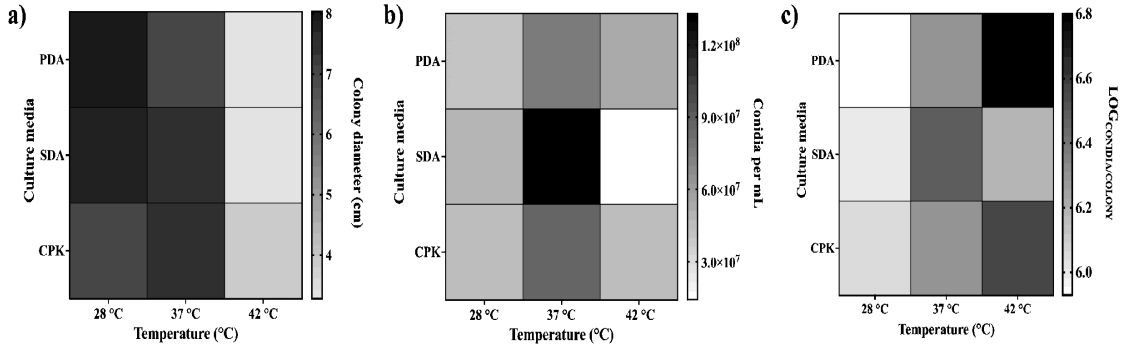

Figure 2. ***Aspergillus flavus*** **growth under different conditions.** ***(a)*** Fungal development is depicted as colony diameter ***(b),*** number of conidia per mL and ***(c),*** the logarithm of the conidia/colony area ratio after 7 days of incubation at various media and temperatures. The darker the box, the higher value. The optimal temperature for the radial growth of *A. flavus* MMe18 is 28 °C, and it decreases as temperature increases, meanwhile conidiation appears to be enhanced, as indicated by calculation of conidiation *per* colony area at 37 °C and 42 °C.

3.3. Temperature Accelerates Conidial Germination of Aspergillus flavus

We showed that temperature affects both the colony size and the conidiation rate of *A. flavus*. To understand how temperature affects conidial germination, we monitored their development over 10 h in liquid medium at three different temperatures. In **Figure 3a** we show that morphological changes associated with germination are present at both 37 °C and 42 °C, within 4 h of incubation, being more pronounced at 37 °C. We observed conidial isotropic growth; they appeared swollen (**S**), and some had already germinated (**G**). In contrast, at 28 °C, these morphological changes were notable only after 6h, with many conidia still in a dormant state (**D**). Furthermore, we observed that hyphal elongation and their intertwining occurred sooner at 37 °C and 42 °C compared to 28 °C. After 8 h of incubation at 37 °C, clusters of conidia were already forming microcolonies with emerging hyphae. At 42 °C, hyphae had begun to intertwine, whereas at 28 °C, the elongation process had only just begun. Germination was also assessed using inocula of $1x10^5$ and $1x10^7$ conidia/mL (**Figure S2**). This was corroborated by determining the germination percentage (**Figure 3b**). At 4 h, 6 h, and 8 h, the germination percentage was significantly higher at 37 °C than at 28 °C, suggesting that 37 °C is the optimal temperature for development. Although incubation at 37 °C favors the germination process, increasing the temperature to 42 °C decreases the germination rate, since after 8 h, there was no significant difference in germination rates between 28 °C and 42 °C. Additionally, the metabolic activity during the germination process was evaluated by MTT method. As shown in **Figure 3c**, the highest absorbance value occurred at 37 °C, indicating that dormancy breaking and germination occur rapidly at this temperature, followed by incubation at 42 °C. Meanwhile, the metabolic activity

 doi:10.20944/preprints202409.1082.v1

of conidia incubated at 28 °C remained low, confirming that the germination process is slower at this temperature.

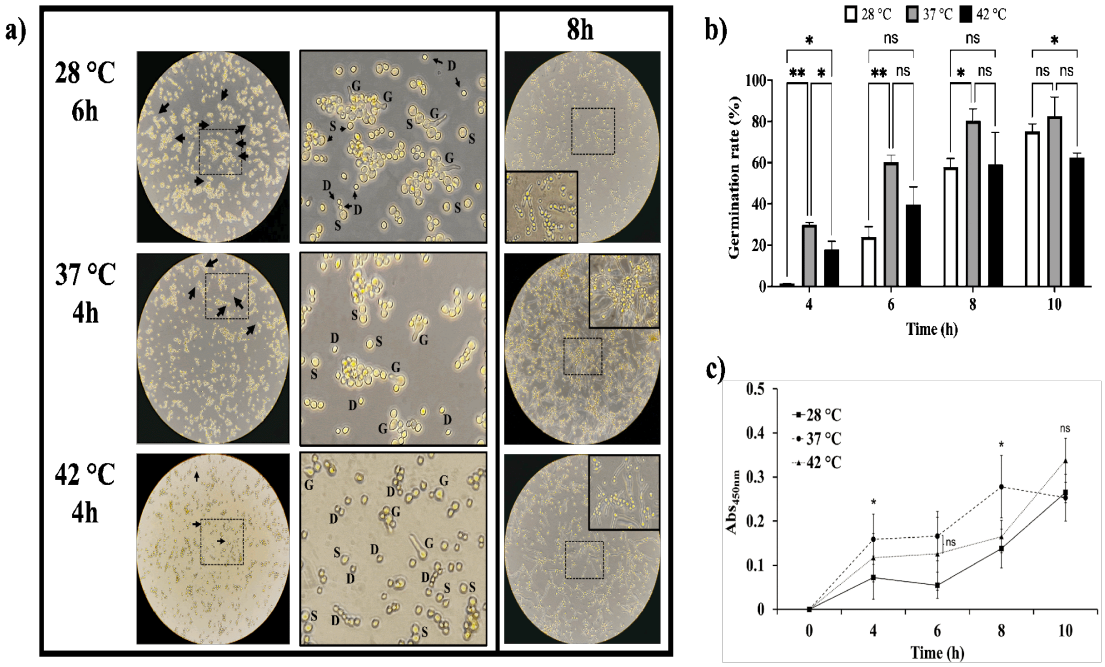

Figure 3. Temperature effect on *A. flavus* conidia germination. The inoculum was adjusted to 1x10^6 conidia/mL in RPMI 1640 medium and seeded onto polystyrene plates, followed by incubation at 28 °C, 37 °C and 42 °C. The figure shows ***a)*** conidial development, highlighting the crucial role of temperature in breaking dormancy and triggering morphological changes such as the swelling (**S**) of dormant conidia (**D**) leading to germination (**G**), solid-line squares represent higher magnification areas within the dotted-line squares; ***b)*** germination percentage and ***c)*** metabolic activity of conidia during the first 10 hours of incubation, emphasizing that increasing temperature stimulates conidial development. Significant differences were determined by two-way ANOVA and Holm-Sidak's multiple comparisons test in both ***b)*** and ***c)*** panels, as indicated [*, p<0.05].

3.4. Aspergillus Flavus In Vitro Biofilm is Favored by Temperature

Biofilm formation is an important virulence factor of opportunistic fungi, so we assessed the ability of *A. flavus* MMe18 to form biofilm and we studied how temperature influences this process. **Figure 4a** depicts biofilm formation at different temperatures: 28 °C (**circles**), 37 °C (**squares**), and 42 °C (**triangles**). A sigmoidal growth pattern was observed in all cases, characterized by a lag phase from 0 to 12 h of incubation, followed by exponential growth that peaked at 48 h at both 28 °C and 42 °C, after which it began to decrease. At 37 °C, biomass continued slightly increasing until 72 h, being the highest biomass value, regardless of the initial fungal inoculum concentration, as observed when biofilm was started with an inoculum concentration of 1x10^5 and 1x10^7 conidia/mL (**Figure S3**). Biofilms were stained with CV and were also examined microscopically. As shown in **Figure 4b**, after 12 h, biofilm morphology was similar across all temperatures, featuring hyphal networks and clusters. Between 24 h and 48 h, hyphal networks became denser, with fewer intercellular spaces and hyphal anastomoses is more pronounced, especially at 37 °C. The increased fungal biomass staining at 37 °C suggests this is the optimal temperature for biofilm formation, which was confirmed by biomass weight measurements presented in **Figure 4c**. We noticed differences in the biomass quantification due to the methodology used, this is more evident at 42 °C.

 doi:10.20944/preprints202409.1082.v1

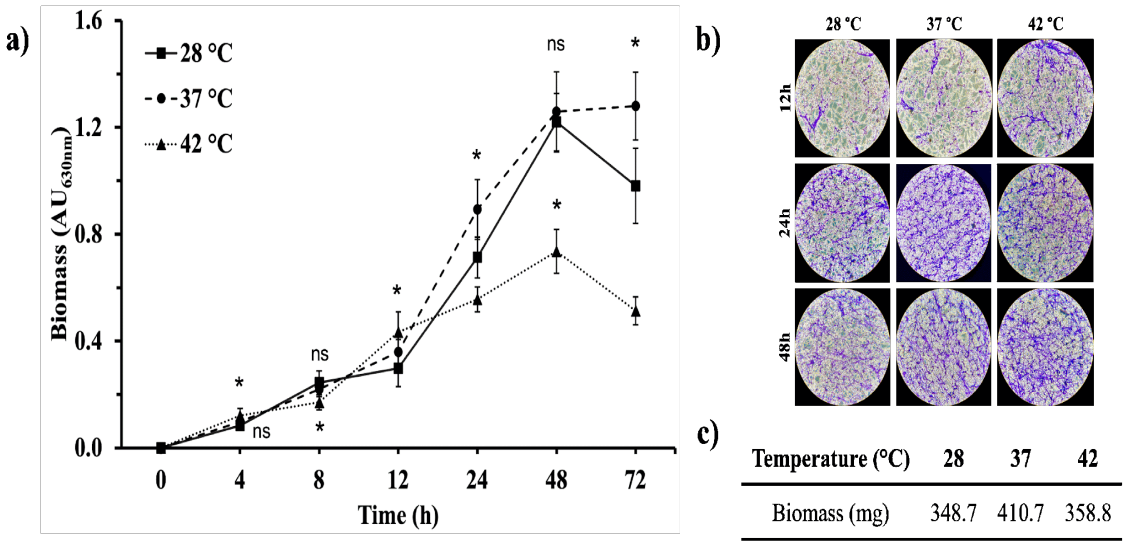

Temperature (°C)	28	37	42
Biomass (mg)	348.7	410.7	358.8

Figure 4. ***Aspergillus flavus*** **MMe18 in vitro biofilm.** Fungal biofilms were established and incubated at different temperatures for 72 h. ***a)*** Biomass was quantified using crystal violet staining across three independent experiments. The values in the graph represent the mean ± SD. Differences between means were assessed using two-way ANOVA followed by Holm-Sidak's multiple comparisons test, with significant differences indicated by [*, $p<0.05$]. Regardless of the development temperature, *A. flavus* biofilm kinetics exhibit a sigmoidal behavior, with well-differentiated phases: initiation (0-12 h), consolidation (12-48 h), mature biofilm (48-72 h) and dispersion (>72 h); ***b)*** At 12, 24, and 48 h, the biofilm was stained with CV and observed at 400x; ***c)*** the biomass of the mature biofilm (48 h) was freeze-dried and weighted, confirming that 37 °C is the optimal temperature for biofilm development and biomass production.

3.5. Architecture of the Aspergillus flavus Biofilm

Scanning electron microscopy (SEM) was employed to study the biofilm formation process of *A. flavus* MMe18 in greater detail, with a focus on understanding how temperature influences its architecture and topology. **Figure 5** shows slight changes in the architecture of the biofilm when it develops at different temperatures. Although it has been described that adhesion of the conidia to the substrate occurs within the first 4 h of incubation, it is evident that higher temperatures accelerate germination, as observed at both 37 °C and 42 °C, confirming the results depicted in **Figure 3a**. The higher magnification in the white boxes shows the surface remodeling process in the conidia as they begin to germinate, losing the hydrophobic protein layer. After 8 h of incubation at 28 °C, some conidia are seen germinating, while at 37 °C and 42 °C, there is already interweaving of hyphae, which is only seen after 12 h when plates are incubated at 28 °C. At 12 h of incubation, the multilayered hyphal network and hyphal anastomoses are evident when plates are incubated at 37 °C and 42 °C. After 24 hours of incubation, a multilayered biofilm is observed at all three temperatures evaluated, with no significant difference in topology or biomass amount, which aligns with the data described in **Figure 4a**. It is only clear that at 37 °C and 42 °C, hyphal anastomosis is more pronounced. According to **Figure 4a**, the maturation phase of the *A. flavus* biofilm is reached after 48 hours of incubation, as corroborated by the analysis of its architecture. At this stage, a multilayered network of hyphae, extensive anastomosis, formation of water channels, low production of exopolymeric substance, and, at 42 °C, a considerable presence of conidial heads and abundant conidia indicate the transition to the dispersion phase, which occurs after 72 h.

 doi:10.20944/preprints202409.1082.v1

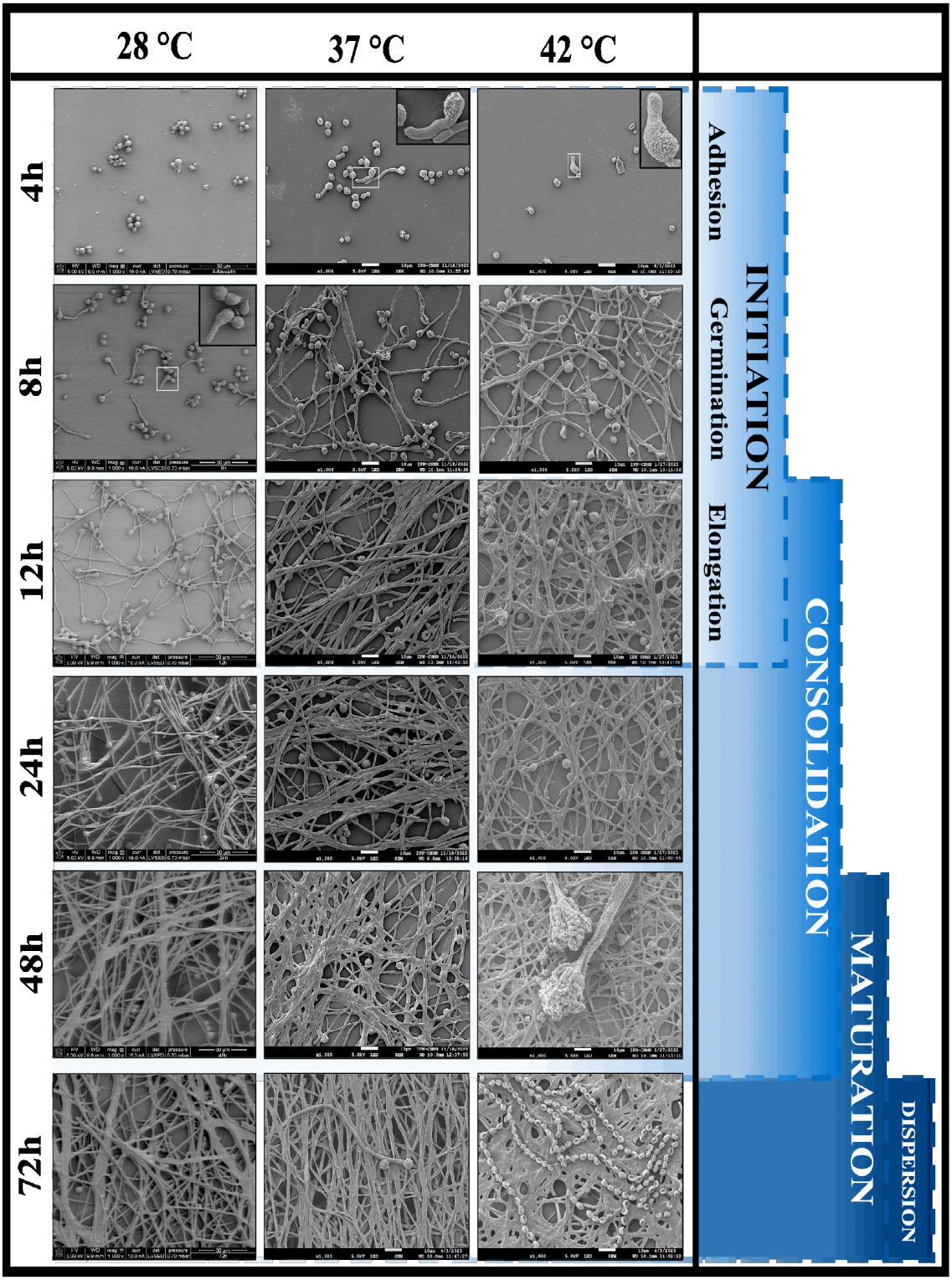

Figure 5. Architecture of *Aspergillus flavus* in vitro biofilm. *A. flavus* biofilm was established and incubated at different temperatures. Its development was monitored for 72 h using scanning electron microscopy. Initiation (0-12 h), involves conidial adhesion to the surface during the first 4 h. Along with this phenomenon, conidial germination takes place at 37 °C and 42 °C but not at 28 °C, and it is evident that breaking dormancy triggers morphological and structural changes on the conidial surface. After 12 h, hyphal elongation is extensive, and they have crisscrossed forming networks. Consolidation (12-48 h), where hyphal networks grow and form a three-dimensional structure that increases its thickness and density, some hyphae have joined by anastomosis and extracellular matrix is secreted as well. At this point, the topology of the biofilm is indistinguishable regardless of the

 doi:10.20944/preprints202409.1082.v1

temperature of development. When the biofilm matures (48 h), its topology is well defined with water channels and a thick multilayer of merged hyphal networks, and only at 42 °C are some conidial heads present. After 72 h, the biofilm has started to lose thickness, preparing for the fungal dispersion (>72 h) and the restart of the cycle. Black line squares represent higher magnification areas within the white line squares. The samples were visualized according to schedule appointments in the CNMN-IPN.

3.6. Biochemical Composition of the Aspergillus flavus Mature Biofilm

We studied the mature biofilm of *A. flavus* MMe18 and compared its biochemical composition at different temperatures using epifluorescence microscopy with two fluorochromes mixtures: **M1** (Calcofluor white + Flamingo™) and **M2** (Concanavalin A + propidium iodide). The upper panel of **Figure 6** shows the labeling of carbohydrates (green) and eDNA (red), using Con A and PI, respectively. Green labeling with concanavalin A is observed on the hyphal and conidial surfaces, as well as in the extracellular matrix (ECM), where the fungal cells are embedded. Red labeling with PI is seen on nucleic acids inside the conidia and some hyphae, where DNA has been released into the intercellular space during the anastomosis process. The co-localization of the two markers indicates the convergence of both biomolecules, observed in the ECM and within the conidia, which appear with a red interior and green surface. There are no apparent changes in the proportion of these biomolecules across the three temperatures evaluated. In the lower section, biofilms labeled with Flamingo™ (green) and calcofluor white (blue) are shown, and we observed a homogeneous proportion of protein and chitin, regardless of the incubation temperature. There is a green label over hyphae and primarily on the conidia, probably due to the hydrophobic protein layer present on the conidial surface, which, as we previously mentioned, is lost when conidia germinates. We also observed the convergence of both fluorochromes in the ECM, particularly in the biofilm developed at 37 °C, where there is a rich presence of carbohydrates.

 doi:10.20944/preprints202409.1082.v1

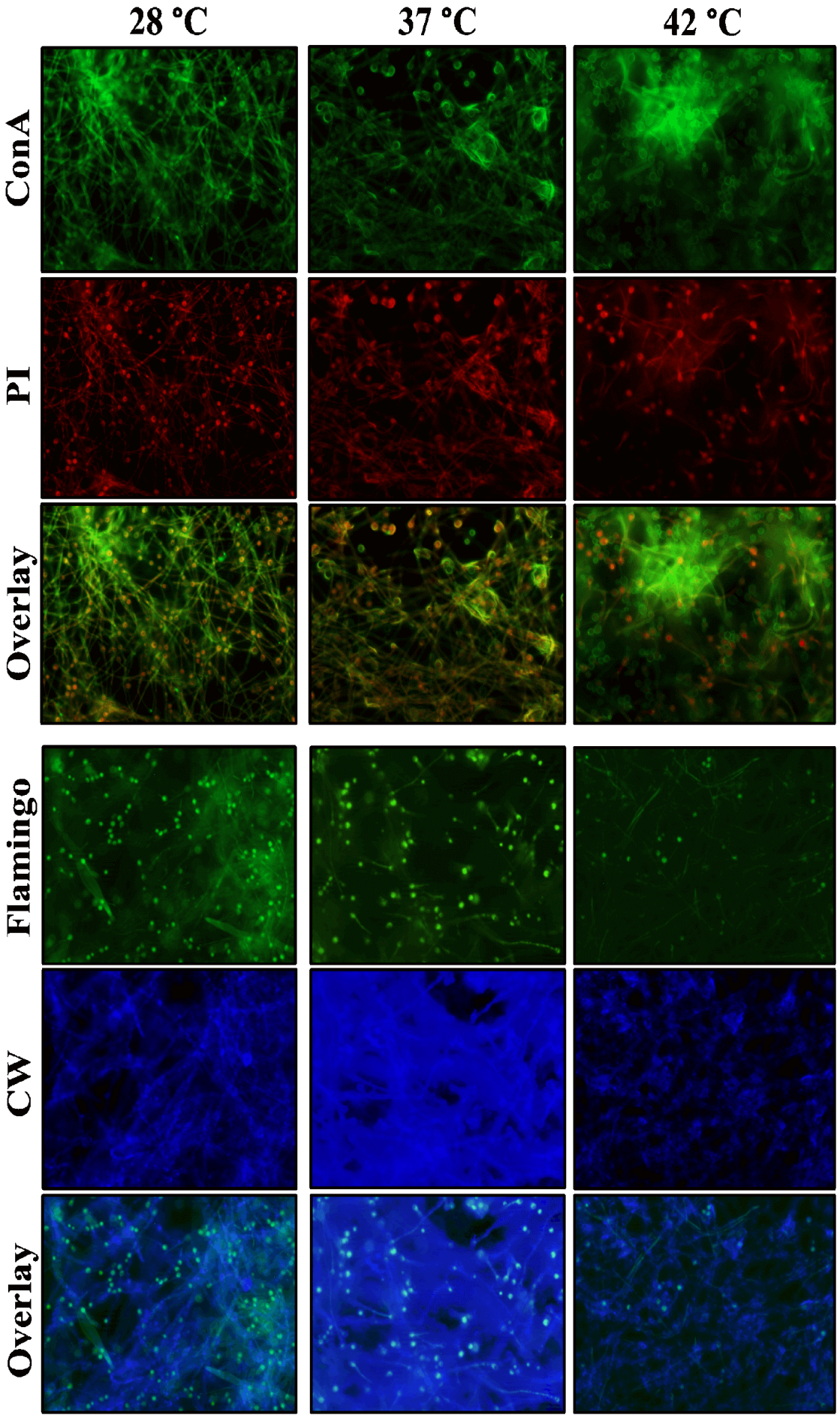

 doi:10.20944/preprints202409.1082.v1

Figure 6. Biomolecules in the in vitro biofilm of *Aspergillus flavus* MMe18. The mature biofilm was stained to visualize the presence of biomolecules and observed using epifluorescence microscopy at 400x total magnification. In the **upper panel**, the fungal biofilm was stained with concanavalin A (green), which binds to glucosyl and mannosyl residues, and propidium iodide (red), which intercalates into DNA. The red stain is observed within hyphae and conidia, and its presence in the extracellular space indicates that the ECM contains eDNA. The green stain is primarily seen on conidial and hyphal surfaces, composed of glucans and mannans, but is also present in the surrounding space, clearly indicating the presence of these molecules in the ECM. In the **lower panel**, the biofilm was stained with Flamingo™ (green) to detect proteins and calcofluor white (blue) to label chitin. The blue stain is abundant due to the presence of chitin in both fungal cells and the ECM. Meanwhile, the green stain is predominantly localized within conidia and, to a lesser extent, inside hyphae and the intercellular space. ***ConA***=*concanavalin A;* ***PI***=*propidium iodide;* ***CW***=*calcofluor white*.

Additionally, dual carbohydrate and lipid labeling was performed on the mature biofilm using a combination of CW and Nile red (NR). **Figure 7** illustrates the labeling of chitin (blue) in the ECM and on the surfaces of hyphae and conidia, contrasted with the lipid labeling by Nile red (orange) within the fungal cells, highlighting the presence of lipid inclusions (**green arrows**). While lipid labeling is prominent inside hyphae and conidia, its presence is practically absent in the intercellular space, except for some specific accumulations. Thus, we infer that its role as a structural component of the ECM of this biofilm is minimal. Although no significant changes associated with the growth temperature were observed, it was noteworthy that these lipid inclusions appear larger in hyphae that developed at 28 °C and become finer when grown at 37 °C and 42 °C. Furthermore, it was also demonstrated by Sudan stain (**lower panel**).

 doi:10.20944/preprints202409.1082.v1

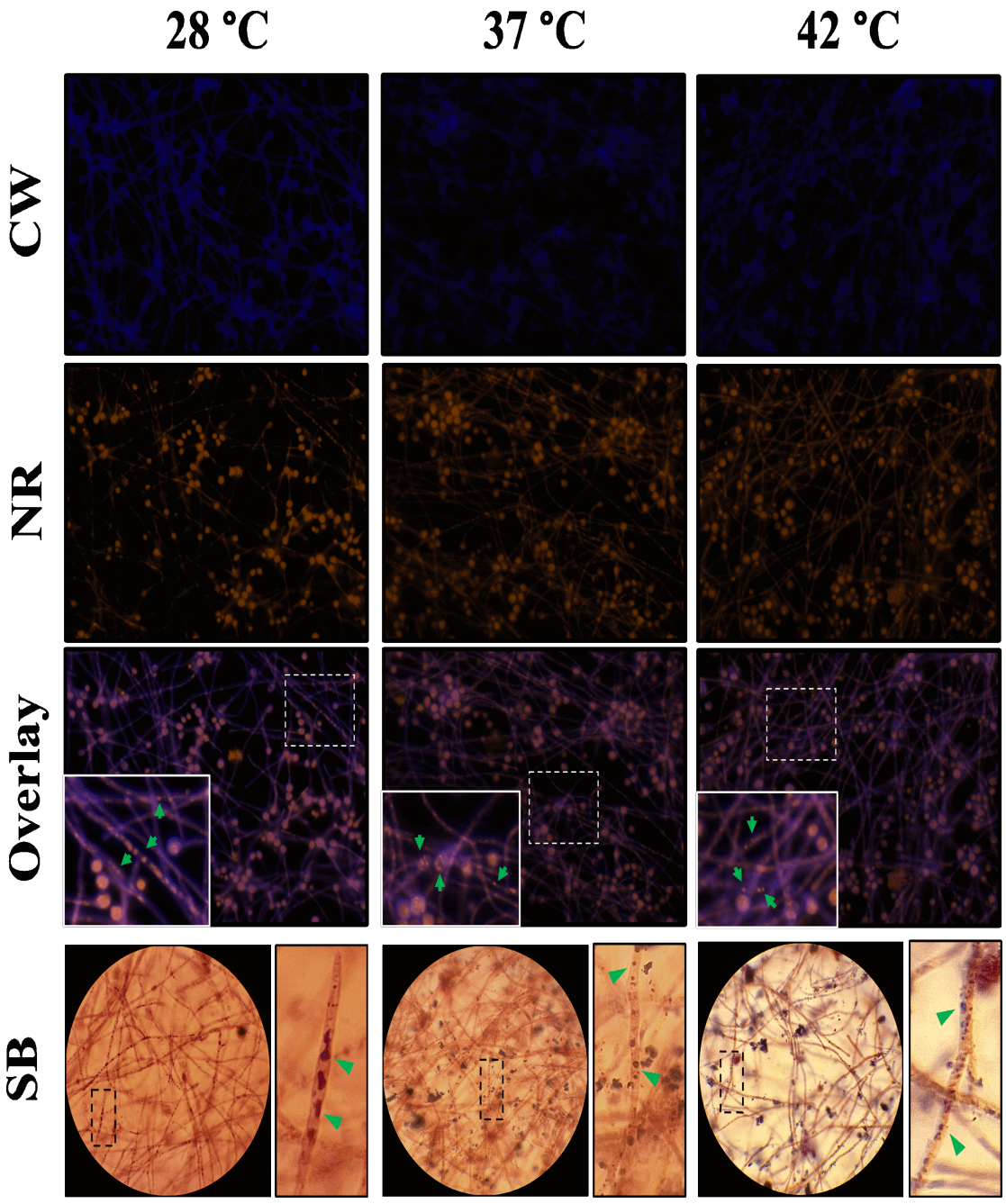

Figure 7. Lipid droplets in the hyphae of *A. flavus* in vitro biofilm. The mature biofilm was stained with calcofluor white (blue) to visualize cell walls and with Nile red (orange) to detect lipids. Samples were observed using epifluorescence microscopy at 400x total magnification (**upper panel**). Additionally, Sudan black B staining was employed and observed under brightfield microscopy at 1000x total magnification (**lower panel**). Lipid staining was observed to a lesser extent in the extracellular matrix, suggesting the minimal structural presence of lipids in the extracellular matrix of *A. flavus* biofilm, with lipids primarily localized within conidia and along hyphae as droplets, highlighted by green arrows. Solid-line squares represent higher magnification areas within the dotted-line squares. ***CW***=*calcofluor white;* ***NR***=*Nile red;* ***SB***=*Sudan black.*

To study the effect of temperature on the density of the mature biofilm we used confocal laser scanning microscopy (CLSM). **Figure 8a** presents the three-dimensional arrangement of the biofilm; when observed at lower magnification, cell density increases with temperature, peaking at 42 °C, followed by growth at 37 °C, and least dense at 28 °C. This is confirmed in the lower panel (**Figure**

 doi:10.20944/preprints202409.1082.v1

8b). In the Z-section of the mature biofilm, it is seen that at 28 °C, the laser penetration is the deepest, with a signal reaching up to 50 µm depth, whereas at 42 °C, it does not exceed 40 µm, and at 37 °C, it does not exceed 30 µm depth. This indicates that the cell density is highest at 37 °C, as inferred from the higher resistance to laser penetration by the biofilm.

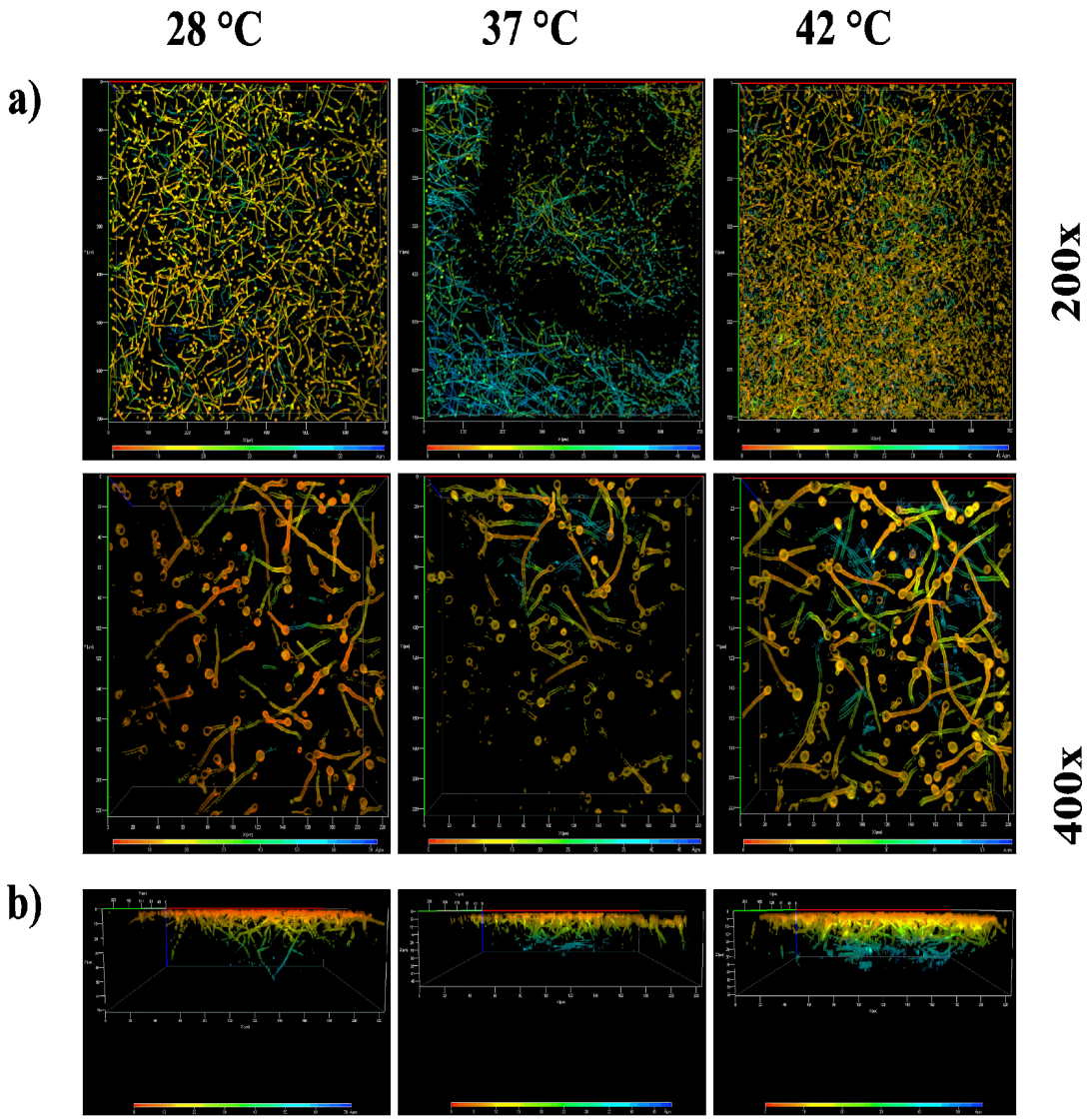

Figure 8. Study of *A. flavus* biofilm cell density and thickness. The mature biofilm was stained with calcofluor white and observed using confocal microscopy. ***a)*** three-dimensional view of the mature biofilm observed at 200x and 400x total magnification. It is evident that hyphal density increases with higher temperatures; ***b)*** Z-stack reconstruction, showing that the cell density limits laser penetration. As depth increases, cell density decreases, indicating a proportional relationship between temperature and cell density, at 37 °C laser penetration power is the lowest.

3.7. Antifungal Susceptibility Profile of A. flavus MMe18 as Planktonic Cells or as Biofilm

In order to study the in vitro antifungal susceptibility profile of this *A. flavus* strain, we assessed the susceptibility of this fungus to some of the routine antifungals used in the treatment of aspergillosis: itraconazole (ITR) and amphotericin B (AMB). We studied whether this profile varies depending on the incubation temperature or during biofilm formation. **Table 1** shows the Minimum Inhibitory Concentration (MIC) values of both antifungals at different temperatures. For ITR, the inhibitory concentration at 28 °C was determined to be 1 µg/mL, while at 37 °C it was 2 µg/mL, and

 doi:10.20944/preprints202409.1082.v1

at 42 °C it was 1 µg/mL again. In the case of AMB, the MIC under the same conditions was 0.0625 µg/mL at 28 °C, 0.25 µg/mL at 37 °C, and 0.0625 µg/mL again at 42 °C. Meanwhile, regardless of the development temperature, the mature fungal biofilm is resistant to either of the two antifungals evaluated, showing MIC values >16 µg/mL.

Table 1. Susceptibility of *Aspergillus flavus* to amphotericin B and itraconazole at different incubation temperatures.

	Amphotericin B (µg/mL)		**Itraconazole (µg/mL)**	
	PK	**BF**	**PK**	**BF**
28 °C	1	>16	0.0625	>16
37 °C	2	>16	0.25	>16
42 °C	1	>16	0.0625	>16

PK=Planktonic cells**; BF**=Mature biofil.m.

4. Discussion

The *Aspergillus* genus comprises ubiquitous fungi, whose medical importance lies in their opportunistic behavior [47]. *A. flavus* is the second most clinically relevant species after *A. fumigatus* [5,7,23], and it is even more prevalent in tropical and subtropical regions with arid climates [48]. Here, we assessed the optimal conditions for growth and biofilm formation of *A. flavus*, emphasizing how temperature affects its development and response to stressors. The isolate MMe18 was identified as *Aspergillus flavus*, sourced from the hospital environment of the "Federico Gómez" Children's Hospital of Mexico. Its growth occurred within 5 to 7 days at 28 °C, with morphological characteristics consistent with the species *A. flavus* (**Figure 1a**, **c**). This included the presence of numerous brown sclerotia, between 500 and 1000 µm in diameter on SDA medium (**Figure 1b**). Accordingly, our *A. flavus* isolate is classified as the L morphotype (>400 µm) [23,49]. Ohkura et al. [50] suggest that the L morphotype is adapted to environments with less microbial competition, where the ability to capture limited nutrients is crucial. Molecular identification confirms the identity of this isolate (**red arrow**), within the *A. flavus*-clade (**green**), which comprises four lineages, primarily *A. flavus* and *A. parasiticus*. This clade is further grouped within the *Flavi* section (**blue**), where *A. tamarii* is also observed. The *A. flavus*- and *A. tamarii*-clades are phylogenetically closely related and, along with the *A. bertholletius*- and *A. nomius*-clades, form a distinct lineage within the *Flavi* section [51]. The development of this fungus in different media was assessed by colony diameter (**Figure 2a**), final conidia concentration (**Figure 2b**) and the logarithm of the ratio of total conidia/colony area (**Figure 2c**). Radial colony growth was inversely proportional to temperature, with measures not exceeding 4 cm at 42 °C, while larger colonies were observed at 28 °C and 37 °C. The highest conidia count was observed in SDA medium incubated at 37 °C, with a final count exceeding $1x10^8$ conidia/mL after 7 days. In the other cases, conidia count remained above $1x10^7$ conidia/mL, even at 42 °C. Furthermore, the conidia/colony ratio increased with temperature, being lower at 28 °C compared to 37 °C and 42 °C. This could be attributed to the thermal stress at higher temperatures, suggesting that conidiation may serve as an optimal dispersion mechanism to ensure fungal survival. This also highlights the capacity of this fungus to proliferate at human physiological temperatures and even higher temperatures, providing an adaptive advantage against the body's defense mechanisms, such as fever. Fever aims to enhance the activity of immune cells and molecules and disrupt the integrity of pathogens and inhibit their growth through thermal stress, which damages proteins, lipids and nucleic acids [52]. The ability to grow at body temperature represents a substantial health risk, particularly for vulnerable hosts such as hemato-oncological patients and those experiencing prolonged neutropenia [53,54]. The size of *A. flavus* conidia enables them to bypass mucociliary clearance and reach the lower airways. Given its ubiquitous presence, nearly everyone is exposed, making *A. flavus* a successful opportunistic pathogen that poses significant risks even at low fungal burdens, particularly to immunocompromised individuals [3,19,55]. In a classic study, Ford & Friedman [56] demonstrated, in a murine model, a correlation between inoculum size

 doi:10.20944/preprints202409.1082.v1

and lethality across various *Aspergillus* species, with 100% lethality observed at $1x10^6$ conidia/mL of *A. flavus*. Moreover, although immunosuppression with corticosteroids exacerbates the disease, it is not necessary for infection establishment. Other authors addressed this. Usman et al. [57] demonstrated that a fungal burden of $1x10^4$ conidia/mL of *A. flavus* causes 80% lethality in *C. elegans* and *G. melonella* while for immunocompetent rabbits, a concentration of 0.75-$1x10^8$ conidia/mL is sufficient for establishing a paranasal infection [58]. Temperature is crucial for microbial adaptation, colonization, and proliferation. The ability to thrive at 37 °C is a common trait of pathogenic microorganisms [21], suggesting a link between growth and germination at this temperature and the pathogenicity of *Aspergillus* species [59]. Therefore, in this study, we assessed the fungus's capacity to grow at higher temperatures, as well as its germination and metabolic activity. **Figure 3a** shows the development of *A. flavus* in liquid medium at 28 °C, 37 °C and 42 °C. Observations were made every 2 h for a total 10 h using an inverted microscope. Conidia incubated at 37 °C began to germinate after 4 hours, coinciding with a higher germination percentage (**Figure 3b**) and the highest values of metabolic activity (**Figure 3c**). This is followed by conidia incubated at 42 °C. In contrast, conidia incubated at 28 °C started germinating up to 6 hours and showing the lowest germination percentage and metabolic activity values throughout the incubation period. Notably, after 8 h of incubation at 37 °C, the germinated conidia began to group into microcolonies, forming the basis of hyphal networks. This behavior was more pronounced with an inoculum of $1x10^5$ conidia/mL (**Figure S2**). Morelli et al. [60] attributes this to thigmotropism, a well-studied phenomenon in plants and phytopathogenic fungi, and already documented in *A. fumigatus* [61]. In an in vivo model of fungal infection using silkworms (*Bombyx mori*), Kumar et al. [62] reported that *A. flavus* conidia germinates after 6 hours and continues up to 12 h post-inoculation with $1x10^6$ conidia/mL, incubating at 26 °C and 80% humidity. These findings are consistent with our in vitro observations. It can be inferred that physiological temperature accelerates the germination of *A. flavus* conidia. The germination process involves the breaking of dormancy, where dormant conidia (***D***) undergo isotropic growth, leading to an increase in size (***S***) and progress to germination (***G***), characterized by the emergence of the germ tube. This is closely influenced by environmental factors such as nutrient availability, temperature and oxygen tension [60,63] and triggers metabolic pathways responsible for cell wall remodeling [64]. Biofilm growth is common in nature. Microorganisms interact within mixed communities enabling them to withstand hostile environmental conditions, including those present within the human body. The role of these microbial consortia in chronic and recalcitrant infections, which are often associated with lower therapeutic success rates, is well-documented [65,66]. To assess the biofilm-forming capacity of this *A. flavus* isolate and determine the optimal conditions, its development was monitored over 72 h, assessing different temperatures and initial conidial densities. **Figure 4a** illustrates the biofilm formation kinetics with an inoculum of $1x10^6$ conidia/mL, incubated at 28 °C (**circles**), 37 °C (**squares**), and 42 °C (**triangles**). The curve exhibits a sigmoidal pattern, characteristic of microbial growth curves, with lag phase between 0 and 12 hours of incubation. At this point, no difference in biomass quantification was observed regardless of the development temperature. When the biofilm is initiated with $1x10^7$ conidia/mL, biomass increase occurs earlier, resulting in an attenuated adaptation phase (**Figure S3**). This is followed by a logarithmic growth phase, observed between 12 and 48 hours. At 48 hours, peak biomass is achieved at 28 °C and 42 °C, after which it declines. In contrast, at 37 °C, the growth rate slows but slightly increases rather than declining. These findings are consistent with Morelli et al. [60], who describe three basic phases of *A. fumigatus* biofilm development: initiation (0-12h), immature (12-24h), mature (>24h). Based on this, we propose the following phases for the *A. flavus* biofilm development: **1. Initiation phase (0-12 h)**: which includes adhesion, germination and the start of filamentation, with a slight increase in biomass; **2. Biofilm consolidation phase (12-48 h)**: characterized by a significant biomass increase due to active hyphal development and the formation of multi-layered networks; **3. Maturation phase (48-72 h)**: the growth rate slows, the biofilm morphology becomes well-structured and defined, and biomass reaches its peak; **4. Dispersion phase (>72 hours)**: marked by biomass abatement and conidial dispersion. It was confirmed by studying the biofilm morphology (**Figure 4b**). After 12 h, hyphal staining was minimal, making the morphology nearly indistinguishable regardless of temperature, with only a slight

 doi:10.20944/preprints202409.1082.v1

increase at 42 °C. At 24 hours, greater staining was observed in the biofilm incubated at 37 °C. Upon maturation, the biomass staining was similar across the assessed temperatures. Additionally, the dry weight of the mature biofilm (**Figure 4c**) shows that the highest biomass was obtained at 37 °C, followed by 42 °C, and the lowest at 28 °C. González-Ramírez et al. [61] compared the biofilm formed by clinical and environmental isolates of *A. fumigatus* incubated at 28 and 37 °C. Both isolates form a mature biofilm within 24 h, with development favored at 28 °C. They attributed the reduced growth at higher temperatures to thermal stress, regardless of the isolate's source. In contrast, our observations suggest that this *A. flavus* isolate may possess adaptive mechanisms enabling it to thrive at higher temperatures, which could aid its establishment in the human body, particularly in hospital environments. It is evident that higher initial inoculum concentrations accelerate biofilm development, resulting in a less defined formation curve, as seen with $1x10^7$ conidia/mL (**Figure S3**). Mowat et al. [67] studied how initial inoculum density affects mature *A. fumigatus* biofilm. They found that higher inoculum concentrations led to reduced biomass and biofilm thickness, poorer filamentation, and increased susceptibility to mechanical damage. Hornby et al. [68] found that inoculum size shapes *Ceratocystis ulmi* development: higher concentrations favor blastoconidia, while lower concentrations promote mycelial growth, attributed to quorum-sensing molecules (QSM) secreted by the fungus. The phenomenon of auto-inhibition prevents conidia from germinating by releasing auto-inhibitors when cell density is very high. We observed a similar effect when evaluating the germination kinetics with an inoculum of $1x10^7$ conidia/mL (**Figure S2**). The biofilm-capacity has been widely studied in *Aspergillus* genus, primarily focused on *A. fumigatus* due to its significant clinical impact [69]. Villena et al. have detailed *A. niger* biofilms, exploring their characteristics and biotechnological applications [70–72]. Our group has characterized biofilms of *A. fumigatus* [61] and *A. terreus* [73]. Although *A. flavus* biofilm has been studied [74–76], no studies to date have provided a comprehensive step-by-step characterization of this process. To our knowledge, this study represents the first attempt to characterize the in vitro biofilm of *A. flavus* using an integrative approach. We used scanning electron microscopy (SEM) to provide a detailed description of the biofilm architecture, as shown in **Figure 5**. After 4 h of incubation, germination occurred at 37 and 42 °C, but at 28 °C, only conidia were visible, consistent with observations in **Figure 3a**. Our analysis showed that germination is faster at 37 and 42 °C than at 28 °C. Higher magnification reveals differences in the surface structure of germinated conidia and germ tubes, attributed to variations in cell wall composition. At this stage, two key events for colonization and biofilm formation are evident: adhesion and germination. Adhesion partially relies on conidial topography and cell wall composition, which mediate hydrophobic and electrostatic interactions with the surface [77]. Villena & Gutiérrez-Correa [72] described how the rough conidial surface of *A. niger* aids initial fungal-substrate contact. During germination, the hydrophobic layer is lost, revealing the hyphal cell wall [64,78,79]. After 8 h, conidia at 28 °C began to germinate, while at 37 and 42 °C, primary hyphal networks formed. At 12 h, a monolayer of hyphae is seen at 28 °C, whereas at 37 and 42 °C, multilayered networks and hyphal junctions forming interhyphal channels mark the onset of biofilm consolidation. At this point, susceptibility to external stressors decreases [60,80]. Between 24 to 48 h, biofilm growth accelerates. SEM images reveal minimal topographical differences across the temperatures, although the biofilms exhibit well-defined characteristics. Multilayering intensifies, hyphal anastomosis is extensive, and interhyphal channels are more evident, along with EPS production, indicating a mature biofilm. At 42 °C, the presence of aspergillary heads is notable due to reduced biofilm formation under nutrient-rich and thermal stress conditions, suggesting that the fungus relies on conidiation and subsequent propagation as survival strategy. It has been reported that some genes involved in conidiogenesis also play roles in stress response signaling pathways [81,82]. Finally, after 72 h of incubation, biofilms at 28 and 42 °C exhibit reduced turgor and thickness, indicating the entry to senescence and dispersion phase. In contrast, at 37 °C, biofilm stratification increases, and germinating conidia are observed. This is consistent with CV biomass quantification, which shows a slight increase at 72 h rather than a decrease (**Figure 4a**). Thus, it is hypothesized that the dispersion phase could extend up to 96 h under these conditions, as observed in *A. terreus* biofilm by Rayón-López et al. [73]. Studying biofilm formation in *Aspergillus* spp., requires considering the

 doi:10.20944/preprints202409.1082.v1

heterogeneity in development times and environmental and nutritional factors influencing the process. *A. fumigatus*, the most clinically significant species in this genus, can develop a mature biofilm within 24 h under optimal conditions, as reported by Mowat et al. [67] and corroborated by our group [43,61]. This rapid biofilm formation likely contributes to its high virulence and prevalence in invasive infections. Other species show significantly longer biofilm maturation periods: *A. nidulans*, requires 72 hours [83], while *A. terreus* may take up to 96 h. *A. niger* shows notable variability, with biofilm maturation occurring as early as 36 h [84] or extending to 96 h under different parameters [71]. This study is the first to detail the in vitro biofilm formation kinetics of *A. flavus*, showing a peak at 48 h, followed by a dispersal phase extending up to 72 h at 37 °C. The composition and functional roles of the extracellular matrix (ECM) in microbial biofilms are key to resistance, preservation, and long-term persistence, making it a significant area of interest [85,86]. Though ECM composition varies between fungi [87], it typically includes four macromolecules classes: carbohydrates and proteins, mainly, as well as lipids and nucleic acids. We employed epifluorescence microscopy to identify ECM molecular constituents. As shown in **Figure 6**, colocalization of fluorochromes around fungal cells revealed the presence of carbohydrates, nucleic acids and proteins in the ECM, consistent with findings in other *Aspergillus* biofilms [61,83,84]. Concanavalin A specifically binds to α-D-mannose and α-D-glucose in glycoconjugates, while calcofluor white stains chitin residues. These carbohydrates are major components of the *Aspergillus* spp. cell wall [78]. Our images show labeling with both fluorochromes within the cells and in extracellular spaces, suggesting that ECM carbohydrates have the same biochemical nature as those in the fungal cell wall. Mitchel et al. [85] noted that while cell wall and ECM components may be similar, polysaccharides differ in size and branching patterns, suggesting they are synthesized through distinct pathways or undergo modifications after cleavage from the cell wall. Fluorescence labeling with Flamingo™ confirmed protein presence in the ECM. Conidia exhibited more intense fluorescence than hyphae, regardless of temperature. This disparity may be due to the hydrophobic protein layer on conidia, which, as mentioned, is shed during germination and hyphal development, leading to distinct chemical composition between conidial and hyphal surfaces [64,88]. A slight increase in Flamingo™ fluorescence was detected in the ECM at 28 °C compared to 37 and 42 °C. Additionally, protein inclusions were observed within hyphae at 28 and 37 °C, but not at 42 °C. Proteins like dipeptidylpeptidase V (DPPV), catalase B (CatB) and ribotoxin (ASPF1) have been identified in the ECM of *A. fumigatus* biofilms [69,89]. Interestingly, in *C. albicans*, proteins involved in amino acid and carbohydrate metabolism may influence the structural and functional profile of ECM polysaccharides [90]. Mosier et al. [91] reported that temperature modifies the proteome of biofilms formed by acid mine drainage (AMD) consortia, composed of bacteria, archaea and filamentous fungi, with an upregulation of proteins related to amino acid transport and metabolism. Similarly, development temperature affects *Clostridium perfringens* biofilm morphology: at 37 °C, an adherent biofilm morphotype is observed, while at 25 °C, the biofilm exhibits a non-adherent phenotype and increased susceptibility to mechanical disruption [92]. A subsequent study found that EPS synthesis is temperature-dependent, serving as a survival strategy under hostile conditions and host colonization [93]. Although temperature's impact on fungal biofilm development has been extensively studied in models such as *C. albicans* [94,95] and *A. fumigatus* [61], little is known about its effects on ECM composition. The presence of eDNA in the ECM was confirmed by propidium iodide staining. eDNA was detected within conidia and hyphae, and more prominently in the intercellular spaces at 37 °C, where it appeared as sticky, diffuse regions colocalizing with glycoconjugates, as described by Shopova et al. [96] in *A. fumigatus*. Although eDNA is a minor ECM component and is mainly consists of non-coding sequences [90,97], it is crucial for cell adhesion and cohesion in the biofilm, enhancing structural stability and resistance to stressors, including antifungals agents [98]. Rajendran et al. [97] showed that eDNA release is phase-dependent, and peaks during the maturation phase, largely as a result of autolysis. In *A. nidulans* biofilm, proteases and chitinases activities are linked to nutritional stress responses [99] and triggered during maturation and senescence. These enzymes degrade ECM polymers and cellular components, supplying alternative carbon and nitrogen sources, as described in bacterial biofilms [100,101]. Around 14-15% of the ECM in fungal biofilms is composed of lipids

 doi:10.20944/preprints202409.1082.v1

[102], with neutral glycerolipids being the most abundant, followed by sphingolipids [90]. Nile red staining confirmed the presence of lipids in the *A. flavus* biofilm (**Figure 7**), with minimal fluorescence detected in the ECM, suggesting that lipids are a minor component of this, consistent with other fungal models. Higher fluorescence was observed within conidia, and abundant lipid droplets (LDs) were noted inside the hyphae (**Figure 7, green arrows**). The size of these LDs varied with temperature, appearing larger at 28 °C, while smaller inclusions were seen at 37 °C and 42 °C, which was confirmed by Sudan Black B stain (**lower panel**), similarly to Nemcová et al. [103], who found that *Metschnikowia* yeasts accumulate lipids more efficiently at 15 °C than at room temperature. Although further research is needed, lipids in the ECM are thought to contribute to structural integrity and surface adhesion [84,104]. LDs are amphipathic lipid membranes encasing neutral lipids like triacylglycerols and sterols and are associated with the endoplasmic reticulum (ER) in fungi [105]. They are involved in various functions, including stress response, apoptosis, and autophagy [106–109], and serve as lipid reservoirs during host invasion and mycorrhizal associations, as well as in toxin production and secretion [110–112] though their role and behavior in biofilm formation remains less understood. Lattif et al. [113] suggested that higher lipid levels during the early biofilm phases of biofilm formation may enhance surface adhesion, and they linked this to the presence of lipid rafts in the fungal membrane. They also proposed that higher concentrations of polar lipids, particularly phospholipids and sphingolipids, in biofilm cells may contribute to increased resistance to antifungal agents in biofilms. Our group has also documented LDs in *A. terreus* biofilm [73], suggesting that this could be associated with its oleaginous behavior [114]. In this context, oleaginous fungi are gaining interest because of their ability to produce and accumulate lipids from various substrates, which has potential biotechnological applications [44,103,115]. As previously mentioned, filamentous fungal biofilms are characterized by multilayered hyphal networks that, along with ECM production, confers resistance to stressors and adverse conditions [29]. **Figure 8** illustrates how temperature affects biofilm density. Higher temperatures result in denser and more compact hyphal networks. This is evidenced by reduced laser penetration during Z-stack imaging when the biofilm develops at 37 °C, something more pronounced at 42 °C, reflecting increased structural integrity at elevated temperatures. This enhanced density and integrity could potentially slow the penetration of antifungal agents, as sequestration of molecules within biofilms has been reported [76,90,116]. In **Table 1** is presented the minimal inhibitory concentration (MIC) of two antifungals against planktonic and biofilm cells of *A. flavus* at different temperatures. Both amphotericin B and itraconazole were effective against planktonic cells, highlighting that the MIC for amphotericin B twofold, and itraconazole threefold at 37 °C compared to 28 and 42 °C. Growth at temperatures higher than optimal may induce environmental stress in microorganisms. Stress-induced mutagenesis, leading to antibiotic-resistant phenotypes, has been reported in thermophilic *Bacillus* species [117]. The impact of temperature on the emergence of resistant phenotypes is of significant interest, particularly in the context of climate change, but remains largely unexplored. Recently, Huang et al. [118] demonstrated that incubating the yeast *Rhodosporidiobolus fluvialis* at 37 °C, induces reactive oxygen species (ROS) production, this causes DNA damage and subsequent mutations, leading to the development of hypervirulent and pan-resistant phenotypes. Conversely, no antifungal activity was observed against mature biofilms at any tested temperature, even at concentration higher than 16 μg/mL. This is consistent with previous studies, which have reported that biofilms display significantly higher MICs than planktonic cells [33,74,80,119–121]. Our group has previously reported that *Fusarium solani* biofilm is less susceptible to antifungal drugs to ultraviolet radiation [40]. The mechanisms underlying biofilm-associated resistance have been extensively studied. Nett et al. [30] found that increased β-1,3 glucan content in *C. albicans* biofilm cells contributes to their structural integrity and resistance to antifungal agents. Rajendran et al. [97] observed that eDNA release from lysed hyphae in *A. fumigatus* contributes to biofilms resistance, whereas, combining DNase with an antifungal agent improves efficacy. Kowalski et al. [32] demonstrated that variations in oxygen tension throughout biofilms contribute to voriconazole and amphotericin B resistance. Cells at the biofilm basal layer can restart growth under favorable

 doi:10.20944/preprints202409.1082.v1

conditions. Similar findings have been reported in *C. albicans*, where persistent cells are known to contribute to antifungal resistance [122].

The next step in our research is to identify the molecular mechanisms involved in conidiation and how they are affected by temperature. Is it a response to heat shock stress? Is it just a mechanism of dispersion? And which other stressful environmental factors are involved in conidiation? Moreover, we would like to know how virulence-associated genes regulation varies with temperature in this model.

We also want to identify the lipids in lipid droplets (LDs) and analyze their role in fungal physiology during biofilm formation. We also aim to investigate how temperature influences their composition, and the expression of genes involved in their biosynthesis and physiology, as well as explore their biotechnological applications.

5. Conclusions

Our findings **confirm** that *A. flavus* is thermotolerant, and its optimal growth is at 28 °C but for biofilm formation is 37 °C. Moreover, we found that high temperatures enhance conidial germination and conidiation, which could favor the fungal dispersion. Conversely, the temperature does not affect the ECM composition of *A. flavus* biofilm, which primarily consists of proteins, carbohydrates and eDNA, highlighting the presence of lipids droplets (LDs) within the hypha. Additionally, biofilm formation significantly increased the MICs of antifungal agents regardless of the temperature.

Supplementary Materials: The following supporting information can be downloaded at the website of this paper posted on Preprints.org. **Figure S1:** Molecular identification of *A. flavus* MMe18 by Neighbor-Joining phylogenetic tree construction based on the partial β-tubulin gene sequence; **Figure S2:** *A. flavus* conidia germination analysis adjusting inoculum at ***a)*** $1x10^5$ conidia/mL and ***b)*** $1x10^7$ conidia/mL; **Figure S3:** Biofilm formation kinetics of *A. flavus* using different inoculum size. ***a)*** inoculum adjusted at $1x10^5$ conidia/mL and ***b)*** $1x10^7$ conidia/mL.

Author Contributions: Conceptualization, A.V.R.-T., N.O.P-R. and J.A.H.-B.; methodology, J.A.H.-B., B.N.S.-O., D.G.R.-R.; validation, A.V.R.-T. and N.O.P-R.; formal analysis, A.V.R.-T., N.O.P-R., J.A.H.-B., L.A.B.-H., A.R.-G.; investigation, J.A.H.-B.; resources, A.V.R.-T., N.O.P-R. and V.M.B.-L.; writing—original draft preparation, J.A.H.-B.; writing—review and editing, A.V.R.-T., N.O.P-R. and J.A.H.-B.; supervision, A.V.R.-T. and N.O.P-R.; project administration, A.V.R.-T. and N.O.P-R.; funding acquisition, A.V.R.-T. All authors have read and agreed to the published version of the manuscript. This work is part of the PhD Thesis of J.A.H.-B.; B.N.S.-O. is a Master Student.

Funding: This research was funded by Secretaría de Investigación y Posgrado - Instituto Politécnico Nacional (SIP 20230236 and SIP 20240616).

Institutional Review Board Statement: Not applicable.

Informed Consent Statement: Not applicable.

Data Availability Statement: Data associated with this study has not been deposited into a publicly available repository and will be made available from the corresponding author on reasonable request.

Acknowledgments: J.A.H.-B. thanks CONAHCyT for his doctoral scholarship (CVU: 932226). We are grateful to MSc Jesús Reséndiz Sánchez, from the Hospital Infantil de México "Federico Gómez" for providing the strain we are working with. We sincerely appreciate the help of Dra. Mayahuel Ortega Avilés and Dr. Hugo Martínez Gutiérrez from Centro de Nanociencias y Micro y Nanotecnologías-IPN. A.V.R.T. is COFAA, EDI and SNI Fellow, N.O.P.; V.M.B.L; D.G.R.R. are SNI Fellows.

Conflicts of Interest: The authors declare no conflicts of interest.

References

1. Viegas, C.; Gomes, B.; Dias, M.; Carolino, E.; Aranha Caetano, L. *Aspergillus* Section *Fumigati* in Firefighter Headquarters. *Microorganisms* **2021**, *9* (10), 2112. https://doi.org/10.3390/microorganisms9102112.
2. Sugui, J. A.; Kwon-Chung, K. J.; Juvvadi, P. R.; Latge, J.-P.; Steinbach, W. J. *Aspergillus fumigatus* and Related Species. *Cold Spring Harb Perspect Med* **2015**, *5* (2), a019786–a019786. https://doi.org/10.1101/cshperspect.a019786.

3. Krishnan, S.; Manavathu, E. K.; Chandrasekar, P. H. *Aspergillus flavus*: An Emerging Non- *fumigatus Aspergillus* Species of Significance. *Mycoses* **2009**, *52* (3), 206–222. https://doi.org/10.1111/j.1439-0507.2008.01642.x.
4. Rudramurthy, S. M.; Paul, R. A.; Chakrabarti, A.; Mouton, J. W.; Meis, J. F. Invasive Aspergillosis by *Aspergillus flavus*: Epidemiology, Diagnosis, Antifungal Resistance, and Management. *JoF* **2019**, *5* (3), 55. https://doi.org/10.3390/jof5030055.
5. Al-Hatmi, A. M. S.; Castro, M. A.; De Hoog, G. S.; Badali, H.; Alvarado, V. F.; Verweij, P. E.; Meis, J. F.; Zago, V. V. Epidemiology of *Aspergillus* Species Causing Keratitis in Mexico. *Mycoses* **2019**, *62* (2), 144–151. https://doi.org/10.1111/myc.12855.
6. Badiee, P.; Alborzi, A.; Nejabat, M. Detection of Aspergillus Keratitis in Ocular Infections by Culture and Molecular Method. *Int Ophthalmol* **2011**, *31* (4), 291–296. https://doi.org/10.1007/s10792-011-9457-5.
7. Lee, C.-Y.; Ho, Y.-J.; Sun, C.-C.; Lin, H.-C.; Hsiao, C.-H.; Ma, D. H.-K.; Lai, C.-C.; Chen, H.-C. Recurrent Fungal Keratitis and Blepharitis Caused by *Aspergillus flavus*. *The American Society of Tropical Medicine and Hygiene* **2016**, *95* (5), 1216–1218. https://doi.org/10.4269/ajtmh.16-0453.
8. Pasqualotto, A. C.; Denning, D. W. An Aspergilloma Caused by *Aspergillus flavus*. *Med Mycol* **2008**, *46* (3), 275–278. https://doi.org/10.1080/13693780701624639.
9. Martinez-Pajares, J. D.; Martinez-Ferriz, M. C.; Moreno-Perez, D.; Garcia-Ramirez, M.; Martin-Carballido, S.; Blanch-Iribarne, P. Management of Obstructive Renal Failure Caused by Bilateral Renal Aspergilloma in an Immunocompetent Newborn. *J Med Microbiol* **2010**, *59* (3), 367–369. https://doi.org/10.1099/jmm.0.012799-0.
10. Singal, A.; Grover, C.; Pandhi, D.; Das, S.; Jain, B. Nosocomial Urinary Tract Aspergilloma in an Immunocompetent Host: An Unusual Occurrence. *Indian J Dermatol* **2013**, *58* (5), 408. https://doi.org/10.4103/0019-5154.117346.
11. Gheisari, M.; Basharzad, N.; Yazdani Charati, J.; Mirenayat, M. S.; Pourabdollah, M.; Ansari, S.; Mortezaee, V.; Abastabar, M.; Jafarzadeh, J.; Haghani, I.; Hedayati, M. T. Galactomannan Detection in Bronchoalveolar Lavage Fluids: A Diagnostic Approach for Fungus Ball in Patients with Pulmonary Tuberculosis? *Mycoses* **2020**, *63* (7), 755–761. https://doi.org/10.1111/myc.13099.
12. Bernardeschi, C.; Foulet, F.; Ingen-Housz-Oro, S.; Ortonne, N.; Sitbon, K.; Quereux, G.; Lortholary, O.; Chosidow, O.; Bretagne, S. Cutaneous Invasive Aspergillosis: Retrospective Multicenter Study of the French Invasive-Aspergillosis Registry and Literature Review. *Medicine* **2015**, *94* (26), e1018. https://doi.org/10.1097/MD.0000000000001018.
13. Singh, S. A.; Dutta, S.; Narang, A.; Vaiphei, K. Cutaneous *Aspergillus flavus* Infection in a Neonate. *Indian J Pediatr* **2004**, *71* (4), 351–352. https://doi.org/10.1007/BF02724105.
14. Merad, Y.; Derrar, H.; Belmokhtar, Z.; Belkacemi, M. *Aspergillus* Genus and Its Various Human Superficial and Cutaneous Features. *Pathogens* **2021**, *10* (6), 643. https://doi.org/10.3390/pathogens10060643.
15. Bhatnagar-Mathur, P.; Sunkara, S.; Bhatnagar-Panwar, M.; Waliyar, F.; Sharma, K. K. Biotechnological Advances for Combating *Aspergillus flavus* and Aflatoxin Contamination in Crops. *Plant Sci* **2015**, *234*, 119–132. https://doi.org/10.1016/j.plantsci.2015.02.009.
16. Alshannaq, A. F.; Gibbons, J. G.; Lee, M.-K.; Han, K.-H.; Hong, S.-B.; Yu, J.-H. Controlling Aflatoxin Contamination and Propagation of *Aspergillus flavus* by a Soy-Fermenting *Aspergillus oryzae* Strain. *Sci Rep* **2018**, *8* (1), 16871. https://doi.org/10.1038/s41598-018-35246-1.
17. Mamo, F. T.; Shang, B.; Selvaraj, J. N.; Wang, Y.; Liu, Y. Isolation and Characterization of *Aspergillus flavus* Strains in China. *J Microbiol.* **2018**, *56* (2), 119–127. https://doi.org/10.1007/s12275-018-7144-1.
18. Wang, P.; Chang, P.-K.; Kong, Q.; Shan, S.; Wei, Q. Comparison of Aflatoxin Production of *Aspergillus flavus* at Different Temperatures and Media: Proteome Analysis Based on TMT. *Int J Food Microbiol* **2019**, *310*, 108313. https://doi.org/10.1016/j.ijfoodmicro.2019.108313.
19. Kwon-Chung, K. J.; Sugui, J. A. *Aspergillus fumigatus*—What Makes the Species a Ubiquitous Human Fungal Pathogen? *PLoS Pathog* **2013**, *9* (12), e1003743. https://doi.org/10.1371/journal.ppat.1003743.
20. Araujo, R.; Rodrigues, A. G. Variability of Germinative Potential among Pathogenic Species of *Aspergillus*. *J Clin Microbiol* **2004**, *42* (9), 4335–4337. https://doi.org/10.1128/JCM.42.9.4335-4337.2004.
21. Bhabhra, R.; Askew, D. S. Thermotolerance and Virulence of *Aspergillus fumigatus*: Role of the Fungal Nucleolus. *Med Mycol* **2005**, *43* (s1), 87–93. https://doi.org/10.1080/13693780400029486.
22. Seyedmousavi, S.; Guillot, J.; Arné, P.; De Hoog, G. S.; Mouton, J. W.; Melchers, W. J. G.; Verweij, P. E. *Aspergillus* and Aspergilloses in Wild and Domestic Animals: A Global Health Concern with Parallels to Human Disease. *Med. Myco.* **2015**, *53* (8), 765–797. https://doi.org/10.1093/mmy/myv067.
23. Hedayati, M. T.; Pasqualotto, A. C.; Warn, P. A.; Bowyer, P.; Denning, D. W. *Aspergillus flavus*: Human Pathogen, Allergen and Mycotoxin Producer. *Microbiology* **2007**, *153* (6), 1677–1692. https://doi.org/10.1099/mic.0.2007/007641-0.
24. Shabeer, S.; Asad, S.; Jamal, A.; Ali, A. Aflatoxin Contamination, Its Impact and Management Strategies: An Updated Review. *Toxins* **2022**, *14* (5), 307. https://doi.org/10.3390/toxins14050307.

25. Hagiwara, D.; Sakamoto, K.; Abe, K.; Gomi, K. Signaling Pathways for Stress Responses and Adaptation in *Aspergillus* Species: Stress Biology in the Post-Genomic Era. *Biosci Biotechnol Biochem* **2016**, *80* (9), 1667–1680. https://doi.org/10.1080/09168451.2016.1162085.
26. Horianopoulos, L. C.; Kronstad, J. W. Chaperone Networks in Fungal Pathogens of Humans. *JoF* **2021**, *7* (3), 209. https://doi.org/10.3390/jof7030209.
27. Hagiwara, D.; Sakai, K.; Suzuki, S.; Umemura, M.; Nogawa, T.; Kato, N.; Osada, H.; Watanabe, A.; Kawamoto, S.; Gonoi, T.; Kamei, K. Temperature during Conidiation Affects Stress Tolerance, Pigmentation, and Trypacidin Accumulation in the Conidia of the Airborne Pathogen *Aspergillus fumigatus*. *PLoS ONE* **2017**, *12* (5), e0177050. https://doi.org/10.1371/journal.pone.0177050.
28. Fabri, J. H. T. M.; Rocha, M. C.; Fernandes, C. M.; Persinoti, G. F.; Ries, L. N. A.; Cunha, A. F. D.; Goldman, G. H.; Del Poeta, M.; Malavazi, I. The Heat Shock Transcription Factor HsfA Is Essential for Thermotolerance and Regulates Cell Wall Integrity in *Aspergillus fumigatus*. *Front. Microbiol.* **2021**, *12*, 656548. https://doi.org/10.3389/fmicb.2021.656548.
29. Ramage, G.; Rajendran, R.; Gutierrez-Correa, M.; Jones, B.; Williams, C. *Aspergillus* Biofilms: Clinical and Industrial Significance. *FEMS Microbiol Lett* **2011**, *324* (2), 89–97. https://doi.org/10.1111/j.1574-6968.2011.02381.x.
30. Nett, J.; Lincoln, L.; Marchillo, K.; Massey, R.; Holoyda, K.; Hoff, B.; VanHandel, M.; Andes, D. Putative Role of β-1,3 Glucans in *Candida albicans* Biofilm Resistance. *Antimicrob Agents Chemother* **2007**, *51* (2), 510–520. https://doi.org/10.1128/AAC.01056-06.
31. Pereira, R.; Santos Fontenelle, R. O.; Brito, E. H. S.; Morais, S. M. Biofilm of *Candida albicans*: Formation, Regulation and Resistance. *J. Appl. Microbiol.* **2021**, *131* (1), 11–22. https://doi.org/10.1111/jam.14949.
32. Kowalski, C. H.; Morelli, K. A.; Schultz, D.; Nadell, C. D.; Cramer, R. A. Fungal Biofilm Architecture Produces Hypoxic Microenvironments That Drive Antifungal Resistance. *Proc. Natl. Acad. Sci. U.S.A.* **2020**, *117* (36), 22473–22483. https://doi.org/10.1073/pnas.2003700117.
33. Seidler, M. J.; Salvenmoser, S.; Müller, F.-M. C. *Aspergillus fumigatus* Forms Biofilms with Reduced Antifungal Drug Susceptibility on Bronchial Epithelial Cells. *Antimicrob Agents Chemother* **2008**, *52* (11), 4130–4136. https://doi.org/10.1128/AAC.00234-08.
34. Garcia-Solache, M. A.; Casadevall, A. Global Warming Will Bring New Fungal Diseases for Mammals. *mBio* **2010**, *1* (1), e00061-10. https://doi.org/10.1128/mBio.00061-10.
35. Parsons, M. G.; Diekema, D. J. What Is New in Fungal Infections? *Modern Pathology* **2023**, *36* (6), 100187. https://doi.org/10.1016/j.modpat.2023.100187.
36. Seidel, D.; Wurster, S.; Jenks, J. D.; Sati, H.; Gangneux, J.-P.; Egger, M.; Alastruey-Izquierdo, A.; Ford, N. P.; Chowdhary, A.; Sprute, R.; Cornely, O.; Thompson, G. R.; Hoenigl, M.; Kontoyiannis, D. P. Impact of Climate Change and Natural Disasters on Fungal Infections. *The Lancet Microbe* **2024**, *5* (6), e594–e605. https://doi.org/10.1016/S2666-5247(24)00039-9.
37. Rodríguez-Tovar, A. V.; Ruiz-Medrano, R.; Herrera-Martínez, A.; Barrera-Figueroa, B. E.; Hidalgo-Lara, M. E.; Reyes-Márquez, B. E.; Cabrera-Ponce, J. L.; Valdés, M.; Xoconostle-Cázares, B. Stable Genetic Transformation of the Ectomycorrhizal Fungus *Pisolithus tinctorius*. *J Microbiol Methods* **2005**, *63* (1), 45–54. https://doi.org/10.1016/j.mimet.2005.02.016.
38. Perera, M.; Wijayarathna, D.; Wijesundera, S.; Chinthaka, M.; Seneviratne, G.; Jayasena, S. Biofilm Mediated Synergistic Degradation of Hexadecane by a Naturally Formed Community Comprising *Aspergillus flavus* Complex and *Bacillus cereus* Group. *BMC Microbiol* **2019**, *19* (1), 84. https://doi.org/10.1186/s12866-019-1460-4.
39. Hedayati, M. T.; Taghizadeh-Armaki, M.; Zarrinfar, H.; Hoseinnejad, A.; Ansari, S.; Abastabar, M.; Er, H.; Özhak, B.; Öğünç, D.; Ilkit, M.; Seyedmousavi, S. Discrimination of *Aspergillus flavus* from *Aspergillus oryzae* by Matrix-assisted Laser Desorption/Ionisation Time-of-flight (MALDI-TOF) Mass Spectrometry. *Mycoses* **2019**, *62* (12), 1182–1188. https://doi.org/10.1111/myc.13010.
40. Córdova-Alcántara, I. M.; Venegas-Cortés, D. L.; Martínez-Rivera, M. Á.; Pérez, N. O.; Rodriguez-Tovar, A. V. Biofilm Characterization of *Fusarium solani* Keratitis Isolate: Increased Resistance to Antifungals and UV Light. *J Microbiol.* **2019**, *57* (6), 485–497. https://doi.org/10.1007/s12275-019-8637-2.
41. Christensen, G. D.; Simpson, W. A.; Younger, J. J.; Baddour, L. M.; Barrett, F. F.; Melton, D. M.; Beachey, E. H. Adherence of Coagulase-Negative Staphylococci to Plastic Tissue Culture Plates: A Quantitative Model for the Adherence of Staphylococci to Medical Devices. *J Clin Microbiol* **1985**, *22* (6), 996–1006. https://doi.org/10.1128/jcm.22.6.996-1006.1985.
42. Peeters, E.; Nelis, H. J.; Coenye, T. Comparison of Multiple Methods for Quantification of Microbial Biofilms Grown in Microtiter Plates. *J Microbiol Methods* **2008**, *72* (2), 157–165. https://doi.org/10.1016/j.mimet.2007.11.010.
43. Ramírez Granillo, A.; Canales, M. G. M.; Espíndola, M. E. S.; Martínez Rivera, M. A.; De Lucio, V. M. B.; Tovar, A. V. R. Antibiosis Interaction of *Staphylococccus aureus* on *Aspergillus fumigatus* Assessed in vitro by Mixed Biofilm Formation. *BMC Microbiol* **2015**, *15* (1), 33. https://doi.org/10.1186/s12866-015-0363-2.

44. M38-A Reference Method for Broth Dilution Antifungal Susceptibility Testing of Filamentous Fungi; Approved Standard.
45. Fortún, J.; Meije, Y.; Fresco, G.; Moreno, S. Aspergilosis. Formas clínicas y tratamiento. *Enferm Infecc Microbiol Clin* **2012**, *30* (4), 201–208. https://doi.org/10.1016/j.eimc.2011.12.005.
46. Pasqualotto, A. C. Differences in Pathogenicity and Clinical Syndromes Due to *Aspergillus fumigatus* and *Aspergillus flavus*. *Med Mycol* **2009**, *47* (s1), S261–S270. https://doi.org/10.1080/13693780802247702.
47. Horn, B. W.; Sorensen, R. B.; Lamb, M. C.; Sobolev, V. S.; Olarte, R. A.; Worthington, C. J.; Carbone, I. Sexual Reproduction in *Aspergillus flavus* Sclerotia Naturally Produced in Corn. *Phytopathology* **2014**, *104* (1), 75–85. https://doi.org/10.1094/PHYTO-05-13-0129-R.
48. Ohkura, M.; Cotty, P. J.; Orbach, M. J. Comparative Genomics of *Aspergillus flavus* S and L Morphotypes Yield Insights into Niche Adaptation. *G3 Genes|Genomes|Genetics* **2018**, *8* (12), 3915–3930. https://doi.org/10.1534/g3.118.200553.
49. Frisvad, J. C.; Hubka, V.; Ezekiel, C. N.; Hong, S.-B.; Nováková, A.; Chen, A. J.; Arzanlou, M.; Larsen, T. O.; Sklenář, F.; Mahakarnchanakul, W.; Samson, R. A.; Houbraken, J. Taxonomy of *Aspergillus* Section *Flavi* and Their Production of Aflatoxins, Ochratoxins and Other Mycotoxins. *Stud Mycol* **2019**, *93* (1), 1–63. https://doi.org/10.1016/j.simyco.2018.06.001.
50. Evans, S. S.; Repasky, E. A.; Fisher, D. T. Fever and the Thermal Regulation of Immunity: The Immune System Feels the Heat. *Nat Rev Immunol* **2015**, *15* (6), 335–349. https://doi.org/10.1038/nri3843.
51. Kousha, M.; Tadi, R.; Soubani, A. O. Pulmonary Aspergillosis: A Clinical Review. *Eur Respir Rev* **2011**, *20* (121), 156–174. https://doi.org/10.1183/09059180.00001011.
52. Sunnetcioglu, A.; Ekin, S.; Erten, R.; Parlak, M.; Esen, R. Endobronchial Aspergilloma: A Case Report. *Respir Med Case Rep* **2016**, *18*, 1–3. https://doi.org/10.1016/j.rmcr.2016.03.001.
53. Boral, H.; Metin, B.; Döğen, A.; Seyedmousavi, S.; Ilkit, M. Overview of Selected Virulence Attributes in *Aspergillus fumigatus, Candida albicans, Cryptococcus neoformans, Trichophyton rubrum,* and *Exophiala dermatitidis*. *Fungal Genet Biol* **2018**, *111*, 92–107. https://doi.org/10.1016/j.fgb.2017.10.008.
54. Ford, S.; Friedman, L. Experimental Study of the Pathogenicity of Aspergilli for Mice. *J Bacteriol* **1967**, *94* (4), 928–933. https://doi.org/10.1128/jb.94.4.928-933.1967.
55. Usman, S.; Du, C.; Qin, Q.; Odiba, A. S.; He, R.; Wang, B.; Jin, C.; Fang, W. Phosphomannose Isomerase Is Involved in Development, Stress Responses, and Pathogenicity of *Aspergillus flavus*. *Microbiol Spectr* **2022**, *10* (5), e02027-22. https://doi.org/10.1128/spectrum.02027-22.
56. Chakrabarti, A.; Jatana, M.; Sharma, S. C. Rabbit as an Animal Model of Paranasal Sinus Mycoses. *Med Mycol* **1997**, *35* (4), 295–297. https://doi.org/10.1080/02681219780001311.
57. Dagenais, T. R. T.; Keller, N. P. Pathogenesis of *Aspergillus Fumigatus* in Invasive Aspergillosis. *Clin Microbiol Rev* **2009**, *22* (3), 447–465. https://doi.org/10.1128/CMR.00055-08.
58. Morelli, K. A.; Kerkaert, J. D.; Cramer, R. A. Aspergillus Fumigatus Biofilms: Toward Understanding How Growth as a Multicellular Network Increases Antifungal Resistance and Disease Progression. *PLoS Pathog* **2021**, *17* (8), e1009794. https://doi.org/10.1371/journal.ppat.1009794.
59. González-Ramírez, A. I.; Ramírez-Granillo, A.; Medina-Canales, M. G.; Rodríguez-Tovar, A. V.; Martínez-Rivera, M. A. Analysis and Description of the Stages of *Aspergillus fumigatus* Biofilm Formation Using Scanning Electron Microscopy. *BMC Microbiol* **2016**, *16* (1), 243. https://doi.org/10.1186/s12866-016-0859-4.
60. Kumar, V.; Singh, G. P.; Babu, A. M. Surface Ultrastructural Studies on the Germination, Penetration and Conidial Development of *Aspergillus flavus* Link : Fries Infecting Silkworm, Bombyx Mori Linn. *Mycopathologia* **2004**, *157* (1), 127–135. https://doi.org/10.1023/B:MYCO.0000012225.79969.29.
61. Úrbez-Torres, J. R.; Bruez, E.; Hurtado, J.; Gubler, W. D. Effect of Temperature on Conidial Germination of *Botryosphaeriaceae* Species Infecting Grapevines. *Plant Dis* **2010**, *94* (12), 1476–1484. https://doi.org/10.1094/PDIS-06-10-0423.
62. Baltussen, T. J. H.; Zoll, J.; Verweij, P. E.; Melchers, W. J. G. Molecular Mechanisms of Conidial Germination in *Aspergillus* spp. *Microbiol Mol Biol Rev* **2020**, *84* (1), e00049-19. https://doi.org/10.1128/MMBR.00049-19.
63. Ciofu, O.; Moser, C.; Jensen, P. Ø.; Høiby, N. Tolerance and Resistance of Microbial Biofilms. *Nat Rev Microbiol* **2022**, *20* (10), 621–635. https://doi.org/10.1038/s41579-022-00682-4.
64. Costa-Orlandi, C.; Sardi, J.; Pitangui, N.; De Oliveira, H.; Scorzoni, L.; Galeane, M.; Medina-Alarcón, K.; Melo, W.; Marcelino, M.; Braz, J.; Fusco-Almeida, A.; Mendes-Giannini, M. Fungal Biofilms and Polymicrobial Diseases. *JoF* **2017**, *3* (2), 22. https://doi.org/10.3390/jof3020022.
65. Mowat, E.; Butcher, J.; Lang, S.; Williams, C.; Ramage, G. Development of a Simple Model for Studying the Effects of Antifungal Agents on Multicellular Communities of *Aspergillus fumigatus*. *Journal Med Microbiol* **2007**, *56* (9), 1205–1212. https://doi.org/10.1099/jmm.0.47247-0.
66. Hornby, J. M.; Jacobitz-Kizzier, S. M.; McNeel, D. J.; Jensen, E. C.; Treves, D. S.; Nickerson, K. W. Inoculum Size Effect in Dimorphic Fungi: Extracellular Control of Yeast-Mycelium Dimorphism in *Ceratocystis ulmi*. *Appl Environ Microbiol* **2004**, *70* (3), 1356–1359. https://doi.org/10.1128/AEM.70.3.1356-1359.2004.

67. Beauvais, A.; Schmidt, C.; Guadagnini, S.; Roux, P.; Perret, E.; Henry, C.; Paris, S.; Mallet, A.; Prévost, M.-C.; Latgé, J. P. An Extracellular Matrix Glues Together the Aerial-Grown Hyphae of *Aspergillus fumigatus*. *Cell Microbiol* **2007**, *9* (6), 1588–1600. https://doi.org/10.1111/j.1462-5822.2007.00895.x.
68. Gamarra, N. N.; Villena, G. K.; Gutiérrez-Correa, M. Cellulase Production by *Aspergillus niger* in Biofilm, Solid-State, and Submerged Fermentations. *Appl Microbiol Biotechnol* **2010**, *87* (2), 545–551. https://doi.org/10.1007/s00253-010-2540-4.
69. Villena, G. K.; Gutierrez-Correa, M. Production of Cellulase by *Aspergillus niger* Biofilms Developed on Polyester Cloth. *Lett Appl Microbiol* **2006**, *43* (3), 262–268. https://doi.org/10.1111/j.1472-765X.2006.01960.x.
70. Villena, G. K.; Gutiérrez-Correa, M. Morphological Patterns of *Aspergillus niger* Biofilms and Pellets Related to Lignocellulolytic Enzyme Productivities. *Lett Appl Microbiol* **2007**, *45* (3), 231–237. https://doi.org/10.1111/j.1472-765X.2007.02183.x.
71. Rayón-López, G.; Carapia-Minero, N.; Medina-Canales, M. G.; García-Pérez, B. E.; Reséndiz-Sánchez, J.; Pérez, N. O.; Rodríguez-Tovar, A. V.; Ramírez-Granillo, A. Lipid-Like Biofilm from a Clinical Brain Isolate of *Aspergillus terreus:* Quantification, Structural Characterization and Stages of the Formation Cycle. *Mycopathologia* **2023**, *188* (1–2), 35–49. https://doi.org/10.1007/s11046-022-00692-z.
72. Fiori, B.; Posteraro, B.; Torelli, R.; Tumbarello, M.; Perlin, D. S.; Fadda, G.; Sanguinetti, M. In vitro Activities of Anidulafungin and Other Antifungal Agents against Biofilms Formed by Clinical Isolates of Different *Candida* and *Aspergillus* Species. *Antimicrob Agents Chemother* **2011**, *55* (6), 3031–3035. https://doi.org/10.1128/AAC.01569-10.
73. Francis, F.; Druart, F.; Mavungu, J. D. D.; De Boevre, M.; De Saeger, S.; Delvigne, F. Biofilm Mode of Cultivation Leads to an Improvement of the Entomotoxic Patterns of Two *Aspergillus* Species. *Microorganisms* **2020**, *8* (5), 705. https://doi.org/10.3390/microorganisms8050705.
74. Wuren, T.; Toyotome, T.; Yamaguchi, M.; Takahashi-Nakaguchi, A.; Muraosa, Y.; Yahiro, M.; Wang, D.-N.; Watanabe, A.; Taguchi, H.; Kamei, K. Effect of Serum Components on Biofilm Formation by *Aspergillus fumigatus* and Other *Aspergillus* Species. *Jpn J Infect Dis* **2014**, *67* (3), 172–179. https://doi.org/10.7883/yoken.67.172.
75. Priegnitz, B.-E.; Wargenau, A.; Brandt, U.; Rohde, M.; Dietrich, S.; Kwade, A.; Krull, R.; Fleißner, A. The Role of Initial Spore Adhesion in Pellet and Biofilm Formation in *Aspergillus niger*. *Fungal Genet Biol* **2012**, *49* (1), 30–38. https://doi.org/10.1016/j.fgb.2011.12.002.
76. Gow, N. A. R.; Latge, J.-P.; Munro, C. A. The Fungal Cell Wall: Structure, Biosynthesis, and Function. *Microbiol Spectr* **2017**, *5* (3), 5.3.01. https://doi.org/10.1128/microbiolspec.FUNK-0035-2016.
77. Wu, M.-Y.; Mead, M. E.; Kim, S.-C.; Rokas, A.; Yu, J.-H. WetA Bridges Cellular and Chemical Development in *Aspergillus flavus*. *PLoS ONE* **2017**, *12* (6), e0179571. https://doi.org/10.1371/journal.pone.0179571.
78. Mowat, E.; Lang, S.; Williams, C.; McCulloch, E.; Jones, B.; Ramage, G. Phase-Dependent Antifungal Activity against *Aspergillus fumigatus* Developing Multicellular Filamentous Biofilms. *J Antimicrob Chemother* **2008**, *62* (6), 1281–1284. https://doi.org/10.1093/jac/dkn402.
79. Cho, H.-J.; Son, S.-H.; Chen, W.; Son, Y.-E.; Lee, I.; Yu, J.-H.; Park, H.-S. Regulation of Conidiogenesis in *Aspergillus flavus*. *Cells* **2022**, *11* (18), 2796. https://doi.org/10.3390/cells11182796.
80. Zhang, J.; Chen, H.; Sumarah, M. W.; Gao, Q.; Wang, D.; Zhang, Y. *veA* Gene Acts as a Positive Regulator of Conidia Production, Ochratoxin A Biosynthesis, and Oxidative Stress Tolerance in *Aspergillus niger*. *J. Agric. Food Chem.* **2018**, *66* (50), 13199–13208. https://doi.org/10.1021/acs.jafc.8b04523.
81. Corrêa-Almeida, C.; Borba-Santos, L. P.; Rollin-Pinheiro, R.; Barreto-Bergter, E.; Rozental, S.; Kurtenbach, E. Characterization of *Aspergillus nidulans* Biofilm Formation and Structure and Their Inhibition by Pea Defensin Psd2. *Front. Mol. Biosci.* **2022**, *9*, 795255. https://doi.org/10.3389/fmolb.2022.795255.
82. Chatterjee, S.; Das, S. Developmental Stages of Biofilm and Characterization of Extracellular Matrix of Manglicolous Fungus *Aspergillus niger* BSC-1. *J Basic Microbiol* **2020**, *60* (3), 231–242. https://doi.org/10.1002/jobm.201900550.
83. Mitchell, K. F.; Zarnowski, R.; Andes, D. R. Fungal Super Glue: The Biofilm Matrix and Its Composition, Assembly, and Functions. *PLoS Pathog* **2016**, *12* (9), e1005828. https://doi.org/10.1371/journal.ppat.1005828.
84. Nett, J. E.; Andes, D. R. Contributions of the Biofilm Matrix to Candida Pathogenesis. *JoF* **2020**, *6* (1), 21. https://doi.org/10.3390/jof6010021.
85. Flemming, H.-C.; Wingender, J. The Biofilm Matrix. *Nat Rev Microbiol* **2010**, *8* (9), 623–633. https://doi.org/10.1038/nrmicro2415.
86. Erwig, L. P.; Gow, N. A. R. Interactions of Fungal Pathogens with Phagocytes. *Nat Rev Microbiol* **2016**, *14* (3), 163–176. https://doi.org/10.1038/nrmicro.2015.21.
87. Reichhardt, C.; Ferreira, J. A. G.; Joubert, L.-M.; Clemons, K. V.; Stevens, D. A.; Cegelski, L. Analysis of the *Aspergillus fumigatus* Biofilm Extracellular Matrix by Solid-State Nuclear Magnetic Resonance Spectroscopy. *Eukaryot Cell* **2015**, *14* (11), 1064–1072. https://doi.org/10.1128/EC.00050-15.
88. Zarnowski, R.; Westler, W. M.; Lacmbouh, G. A.; Marita, J. M.; Bothe, J. R.; Bernhardt, J.; Lounes-Hadj Sahraoui, A.; Fontaine, J.; Sanchez, H.; Hatfield, R. D.; Ntambi, J. M.; Nett, J. E.; Mitchell, A. P.; Andes, D.

R. Novel Entries in a Fungal Biofilm Matrix Encyclopedia. *mBio* **2014**, *5* (4), e01333-14. https://doi.org/10.1128/mBio.01333-14.

89. Mosier, A. C.; Li, Z.; Thomas, B. C.; Hettich, R. L.; Pan, C.; Banfield, J. F. Elevated Temperature Alters Proteomic Responses of Individual Organisms within a Biofilm Community. *The ISME Journal* **2015**, *9* (1), 180–194. https://doi.org/10.1038/ismej.2014.113.
90. Obana, N.; Nakamura, K.; Nomura, N. A Sporulation Factor Is Involved in the Morphological Change of *Clostridium perfringens* Biofilms in Response to Temperature. *J Bacteriol* **2014**, *196* (8), 1540–1550. https://doi.org/10.1128/JB.01444-13.
91. Obana, N.; Nakamura, K.; Nomura, N. Temperature-Regulated Heterogeneous Extracellular Matrix Gene Expression Defines Biofilm Morphology in *Clostridium perfringens*. *npj Biofilms Microbiomes* **2020**, *6* (1), 29. https://doi.org/10.1038/s41522-020-00139-7.
92. Casagrande Pierantoni, D.; Corte, L.; Casadevall, A.; Robert, V.; Cardinali, G.; Tascini, C. How Does Temperature Trigger Biofilm Adhesion and Growth in *Candida albicans* and Two Non- *Candida albicans Candida* Species? *Mycoses* **2021**, *64* (11), 1412–1421. https://doi.org/10.1111/myc.13291.
93. Pumeesat, P.; Muangkaew, W.; Ampawong, S.; Luplertlop, N. *Candida albicans* Biofilm Development under Increased Temperature. New Microbiol **2017**, 40(4), 279-283.
94. Shopova, I.; Bruns, S.; Thywissen, A.; Kniemeyer, O.; Brakhage, A. A.; Hillmann, F. Extrinsic Extracellular DNA Leads to Biofilm Formation and Colocalizes with Matrix Polysaccharides in the Human Pathogenic Fungus *Aspergillus fumigatus*. *Front. Microbiol.* **2013**, *4*. https://doi.org/10.3389/fmicb.2013.00141.
95. Rajendran, R.; Williams, C.; Lappin, D. F.; Millington, O.; Martins, M.; Ramage, G. Extracellular DNA Release Acts as an Antifungal Resistance Mechanism in Mature *Aspergillus fumigatus* Biofilms. *Eukaryot Cell* **2013**, *12* (3), 420–429. https://doi.org/10.1128/EC.00287-12.
96. Martins, M.; Henriques, M.; Lopez-Ribot, J. L.; Oliveira, R. Addition of DNase Improves the in vitro Activity of Antifungal Drugs against *Candida albicans* Biofilms. *Mycoses* **2012**, *55* (1), 80–85. https://doi.org/10.1111/j.1439-0507.2011.02047.x.
97. Emri, T.; Molnár, Z.; Szilágyi, M.; Pócsi, I. Regulation of Autolysis in *Aspergillus nidulans. Appl Biochem Biotechnol* **2008**, *151* (2–3), 211–220. https://doi.org/10.1007/s12010-008-8174-7.
98. Karygianni, L.; Ren, Z.; Koo, H.; Thurnheer, T. Biofilm Matrixome: Extracellular Components in Structured Microbial Communities. *Trends Microbiol* **2020**, *28* (8), 668–681. https://doi.org/10.1016/j.tim.2020.03.016.
99. Thi, M. T. T.; Wibowo, D.; Rehm, B. H. A. *Pseudomonas aeruginosa* Biofilms. *IJMS* **2020**, *21* (22), 8671. https://doi.org/10.3390/ijms21228671.
100. Reichhardt, C.; Stevens, D. A.; Cegelski, L. Fungal Biofilm Composition and Opportunities in Drug Discovery. *Future Med. Chem.* **2016**, *8* (12), 1455–1468. https://doi.org/10.4155/fmc-2016-0049.
101. Němcová, A.; Szotkowski, M.; Samek, O.; Cagáňová, L.; Sipiczki, M.; Márová, I. Use of Waste Substrates for the Lipid Production by Yeasts of the Genus *Metschnikowia*—Screening Study. *Microorganisms* **2021**, *9* (11), 2295. https://doi.org/10.3390/microorganisms9112295.
102. Andrews, J. S.; Rolfe, S. A.; Huang, W. E.; Scholes, J. D.; Banwart, S. A. Biofilm Formation in Environmental Bacteria Is Influenced by Different Macromolecules Depending on Genus and Species. *Environ Microbiol* **2010**, *12* (9), 2496–2507. https://doi.org/10.1111/j.1462-2920.2010.02223.x.
103. Kuroiwa, T.; Ohnuma, M.; Imoto, Y.; Misumi, O.; Fujiwara, T.; Miyagishima, S.; Sumiya, N.; Kuroiwa, H. Lipid Droplets of Bacteria, Algae and Fungi and a Relationship between Their Contents and Genome Sizes as Revealed by BODIPY and DAPI Staining. *cytologia* **2012**, *77* (3), 289–299. https://doi.org/10.1508/cytologia.77.289.
104. Graef, M. Lipid Droplet-mediated Lipid and Protein Homeostasis in Budding Yeast. *FEBS Letters* **2018**, *592* (8), 1291–1303. https://doi.org/10.1002/1873-3468.12996.
105. Hapala, I.; Griac, P.; Holic, R. Metabolism of Storage Lipids and the Role of Lipid Droplets in the Yeast *Schizosaccharomyces pombe*. *Lipids* **2020**, *55* (5), 513–535. https://doi.org/10.1002/lipd.12275.
106. Péter, M.; Glatz, A.; Gudmann, P.; Gombos, I.; Török, Z.; Horváth, I.; Vígh, L.; Balogh, G. Metabolic Crosstalk between Membrane and Storage Lipids Facilitates Heat Stress Management in *Schizosaccharomyces pombe. PLoS ONE* **2017**, *12* (3), e0173739. https://doi.org/10.1371/journal.pone.0173739.
107. Schepers, J.; Behl, C. Lipid Droplets and Autophagy—Links and Regulations from Yeast to Humans. *J of Cellular Biochemistry* **2021**, *122* (6), 602–611. https://doi.org/10.1002/jcb.29889.
108. Hanano, A.; Alkara, M.; Almousally, I.; Shaban, M.; Rahman, F.; Hassan, M.; Murphy, D. J. The Peroxygenase Activity of the *Aspergillus flavus* Caleosin, AfPXG, Modulates the Biosynthesis of Aflatoxins and Their Trafficking and Extracellular Secretion via Lipid Droplets. *Front. Microbiol.* **2018**, *9*, 158. https://doi.org/10.3389/fmicb.2018.00158.
109. Kobae, Y.; Gutjahr, C.; Paszkowski, U.; Kojima, T.; Fujiwara, T.; Hata, S. Lipid Droplets of Arbuscular Mycorrhizal Fungi Emerge in Concert with Arbuscule Collapse. *Plant Cell Physiol* **2014**, *55* (11), 1945–1953. https://doi.org/10.1093/pcp/pcu123.

110. Qin, P.; Wang, Z.; Lu, D.; Kang, H.; Li, G.; Guo, R.; Zhao, Y.; Han, R.; Ji, B.; Zeng, Y. Neutral Lipid Content in Lipid Droplets: Potential Biomarker of Cordycepin Accumulation in Cordycepin-Producing Fungi. *Molecules* **2019**, *24* (18), 3363. https://doi.org/10.3390/molecules24183363.
111. Lattif, A. A.; Mukherjee, P. K.; Chandra, J.; Roth, M. R.; Welti, R.; Rouabhia, M.; Ghannoum, M. A. Lipidomics of *Candida albicans* Biofilms Reveals Phase-Dependent Production of Phospholipid Molecular Classes and Role for Lipid Rafts in Biofilm Formation. *Microbiology* **2011**, *157* (11), 3232–3242. https://doi.org/10.1099/mic.0.051086-0.
112. Srinivasan, N.; Thangavelu, K.; Uthandi, S. Lovastatin Production by an Oleaginous Fungus, *Aspergillus terreus* KPR12 Using Sago Processing Wastewater (SWW). *Microb Cell Fact* **2022**, *21* (1), 22. https://doi.org/10.1186/s12934-022-01751-2.
113. Kamoun, O.; Ayadi, I.; Guerfali, M.; Belghith, H.; Gargouri, A.; Trigui-Lahiani, H. *Fusarium verticillioides* as a Single-Cell Oil Source for Biodiesel Production and Dietary Supplements. *PSEP* **2018**, *118*, 68–78. https://doi.org/10.1016/j.psep.2018.06.027.
114. Papanikolaou, S.; Dimou, A.; Fakas, S.; Diamantopoulou, P.; Philippoussis, A.; Galiotou-Panayotou, M.; Aggelis, G. Biotechnological Conversion of Waste Cooking Olive Oil into Lipid-Rich Biomass Using *Aspergillus* and *Penicillium* Strains: Waste Oil Valourization by Higher Fungi. *J App Microbiol* **2011**, *110* (5), 1138–1150. https://doi.org/10.1111/j.1365-2672.2011.04961.x.
115. Nett, J. E.; Sanchez, H.; Cain, M. T.; Andes, D. R. Genetic Basis of *Candida* Biofilm Resistance Due to Drug-Sequestering Matrix Glucan. *J INFECT DIS* **2010**, *202* (1), 171–175. https://doi.org/10.1086/651200.
116. Suzuki, H.; Taketani, T.; Kobayashi, J.; Ohshiro, T. Antibiotic Resistance Mutations Induced in Growing Cells of *Bacillus*-Related Thermophiles. *J Antibiot* **2018**, *71* (3), 382–389. https://doi.org/10.1038/s41429-017-0003-1.
117. Huang, J.; Hu, P.; Ye, L.; Shen, Z.; Chen, X.; Liu, F.; Xie, Y.; Yu, J.; Fan, X.; Xiao, M.; Tsui, C. K. M.; Wang, W.; Li, Y.; Zhang, G.; Wong, K. H.; Cai, L.; Bai, F.; Xu, Y.; Wang, L. Pan-Drug Resistance and Hypervirulence in a Human Fungal Pathogen Are Enabled by Mutagenesis Induced by Mammalian Body Temperature. *Nat Microbiol* **2024**, *9* (7), 1686–1699. https://doi.org/10.1038/s41564-024-01720-y.
118. Chandra, J.; Kuhn, D. M.; Mukherjee, P. K.; Hoyer, L. L.; McCormick, T.; Ghannoum, M. A. Biofilm Formation by the Fungal Pathogen *Candida albicans* : Development, Architecture, and Drug Resistance. *J Bacteriol* **2001**, *183* (18), 5385–5394. https://doi.org/10.1128/JB.183.18.5385-5394.2001.
119. Fattahi, M.; Ghasemi, R.; Pinegina, O.; Bahrami, M. M.; Hosseini, M.; Lotfali, E. Effect of Voriconazole on Biofilm of Filamentous Species Isolated from Keratitis. *Arch Clin Infect Dis* **2022**, *16* (6). https://doi.org/10.5812/archcid-122452.
120. Turan, H.; Demirbilek, M. Biofilm-Forming Capacity of Blood–Borne *Candida albicans* Strains and Effects of Antifungal Agents. *Rev Argent Microbiol* **2018**, *50* (1), 62–69. https://doi.org/10.1016/j.ram.2017.05.003.
121. LaFleur, M. D.; Kumamoto, C. A.; Lewis, K. *Candida albicans* Biofilms Produce Antifungal-Tolerant Persister Cells. *Antimicrob Agents Chemother* **2006**, *50* (11), 3839–3846. https://doi.org/10.1128/AAC.00684-06.